Geo-information Science and Remote Sensing

Thesis Report GIRS-2024-51

EXPLORING LASER-INDUCED FLUORESCENCE

An experimental approach towards the remote application of laser-induced fluorescence in vegetation monitoring

Annemieke E. Verhoek

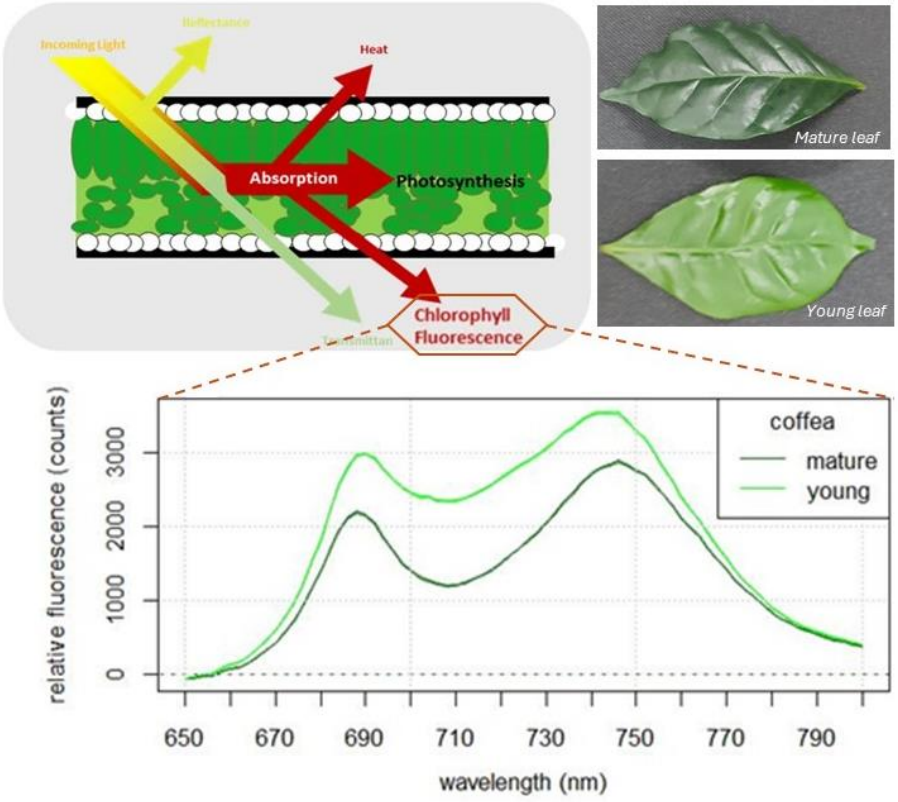

May 15, 2024

WAGENINGEN
UNIVERSITY & RESEARCH

EXPLORING LASER-INDUCED FLUORESCENCE
An experimental approach towards the remote application of laser-induced fluorescence in vegetation monitoring

Annemieke E. Verhoek

Registration number: 1169157

Supervisors:

Prof.Dr.ir. Lammert Kooistra
Dr.ir. Hasib Mustafa

A thesis submitted in partial fulfilment of the degree of Master of Science
at Wageningen University and Research,
The Netherlands.

May 15, 2024
Wageningen, The Netherlands

Thesis code number: GRS-80436
Thesis Report: GIRS-2024 -51
Wageningen University and Research
Laboratory of Geo-Information Science and Remote Sensing

Acknowledgements

I would like to express my sincere gratitude to my supervisors, Lammert Kooistra and Hasib Mustafa, for guiding me throughout the process and providing the help and feedback that I needed. Thank you both for your endless enthusiasm and inspiration throughout the process. Next to that, I want to thank the lab managers of Phenomea, Marcel Staal and Gerard Leentfaar, for providing access to the optics lab, and taking care of the plants over the Christmas break.

Furthermore, I want to thank my friends in the thesis room for their support, inspirational conversations, and, of course, the countless coffee breaks.

Lastly, many thanks to my partner and my family for their endless support and encouragement during this process.

Table of contents

1. Introduction

The growing world population and the changing climate increases the stress on natural resources to provide ourselves access to clean water and food. Extreme weather events, pest and diseases lay an immense pressure on the current day food security. Additionally, natural areas are under pressure as well, diminishing the ecosystem services that these areas provide (Cord et al., 2017; Li et al., 2022). Vegetation health is of great importance not only in relation to food security but for ecosystem services as well.

Remote sensing is a widely applied technology to monitor our earth surfaces. The increasing amount of available and accessible data, in an increasing spatial as well as temporal resolution, enables us to measure and monitor the status of the earth, and is used to monitor deforestation, air pollution, urban sprawl and vegetation health.

Monitoring vegetation health and density is already widely applied and used for different purposes, such as real time identification of deforestation, identifying and monitoring crop health. Meaningful information is extracted from indices such as Normalized Difference Vegetation Index (NDVI) or spectral vegetation indices (VI), calculated from different reflectance bands of the electromagnetic spectrum. These indices often indicate something about the greenness of the surface that is sensed (Du et al., 2017). However, optical spectral reflectances do not tell anything about e.g., photosynthetic processes or biochemical composition or concentrations in vegetation (Du et al., 2017).

As an alternative, this information can be retrieved using fluorescent properties of vegetation. Fluorescence is the emission of light of a substance after absorption of electromagnetic radiation (Zhao et al., 2020). Autofluorescent molecules are found in vegetation, such as lignin and chlorophyll (Donaldson, 2020). Particularly the fluorescent characteristic of chlorophyll has been widely used to evaluate plant health, photosynthetic processes and activity, and responses to environmental stressors (Donaldson, 2020; Guidi et al., 2019; Zhao et al., 2020).

Sun-induced fluorescence (SIF) is a recent development within the domain of remote sensing that is widely applied to the monitoring of vegetation health. Since the sun is a broadband light source, the fluorescence signal that can be retrieved from SIF is in the red and near infra-red part of the spectrum, and can tell something about photosynthetic activity of vegetation (Cogliati et al., 2015). However, the passive sensing of fluorescence gives a weak signal and detection of fluorescence using Fraunhofer lines is needed to extract useful information about chlorophyll fluorescence (Cogliati et al., 2015; Smorenburg et al., 2002).

Laser-induced fluorescence (LIF) is an active form of sensing. Here, fluorescence is generated by using a monochromatic light source, e.g. laser, as excitation source (Zhao et al., 2020). LIF sensing is applied in different domains such as environmental analysis, biochemistry and medicine (Fang et al., 2016; Taylor & Lai, 2021). Because autofluorescent molecules in vegetation are common, LIF is also applied in research about plant physiology, species differentiation, photosynthetic activity and chemical compound concentrations, such as nitrogen (Leufen et al., 2014; Lichtenthaler et al., 1986; Yang et al., 2016, 2018).

Available remote sensing studies present a plethora of topics that use LIF as measurement technique, applied to vegetation. This includes, but is not limited to, topics such as nitrogen estimation of rice (Du et al., 2017, 2020; Yang et al., 2018), the effect of stressors like fungi, nitrogen deficit and water deficit on vegetation (Kharcheva, 2014; Leufen et al., 2014), difference of fluorescence spectra between species (Fedotov et al., 2017), using fluorescence spectra for classification of different species (Yang et al., 2016), and adding a spatial aspect to fluorescence by mapping or combining fluorescence data with 3-d point-cloud data (Lednev et al., 2022a; Wang et al., 2018; Zhao et al., 2020).

A review by Fernandez-Jaramillo et al. (2012) shows that for the excitation source, not one wavelength in particular is often used. On one hand, it is argued that the choice of the excitation light sources differs between different studies because the fluorescence response depends on the subject and the kind of stressor that is investigated (Fernandez-Jaramillo et al., 2012). On the other hand, it is argued that often an ultra-violet excitation source is chosen as it returns a large fluorescence spectrum and thus giving more insight in the plant fluorescence (Wang et al., 2018; Yang et al., 2016; Zhao et al., 2020). However, limited availability and the high cost of UV-laser sources reduce the accessibility of UV LIF excitation (Shamsi et al., 2023). Overall, the costs of the application limits the use of LIF in monitoring vegetation in general (Zhang et al., 2019).

Furthermore, the parameters used in chlorophyll fluorescence (ChlF) studies range from a quantification of chlorophyll content to estimation of photosynthetic activity and efficiency (Lichtenthaler et al., 1986, 2005). The different parameters give various understandings of the physiology and processes in vegetation. However, Fernandez-Jaramillo et al. (2012) argues that a different excitation source leads to a different fluorescent reaction. Therefore, the use of the same ratio for different excitation sources might lead to an incorrect understanding of the meaning of the fluorescent signal.

Lastly, the distance between the target (e.g., leaf, plant) and the sensor as described in literature differs from leaf level (Kharcheva, 2014; Leufen et al., 2014) to remote sensing using a drone Lednev et al., 2022a; Wang et al., 2018). Still, the most common method of LIF sensing is in a lab set-up from close proximity, whereas LIF applications from a remote distance are still lacking.

Therefore, there is a need for a cost-effective set-up to make LIF more accessible for operational vegetation monitoring, complemented with a better understanding of the interpretation of the LIF response of vegetation. This way, a more accessible and accurate way of using LIF can be implemented in the remote sensing domain that will improve our understanding of physiological and biological key parameters in vegetation.

The aim of this research is to develop and evaluate a cost-effective experimental LIF set-up that read-out the fluorescence response of the vegetation and explore the applicability of this set-up at a remote distance and relate the acquired spectra to plant physiology, in order to provide a meaningful interpretation of LIF yielded values. Therefore, the following research questions (RQ) are formulated:

1. Based on literature, what are the most optimal conditions and experimental set-up to research laser induced fluorescence of vegetation?
2. What information can be derived from the LIF measurements that relate to plant physiology?
3. What is the relationship between spectroscopic measurements and plant physiology?
4. To what extent can the LIF set-up be implemented in real-world scenarios?

To answer the RQs, an experimental approach is taken. First, a literature review is conducted to have a better understanding of the current conditions and approaches in LIF research on vegetation. Based on that, various experiments are designed addressing different aspects related to the RQs. Details of the experimental approach and methods are discussed chapter 2.

2. Literature review

This literature review aims to identify the current applications of LIF in research and explore the conditions taken into consideration in literature. This way, the literature review will give an overview of current practices and thus set the foundation for the experimental approach of this research.

To do this, first, a deeper understanding of vegetation fluorescence is explained, to understand the methodological approached used. After that, the qualification and quantification methods used in LIF research are explained. Next, different experimental conditions are discussed, followed by common uses of vegetation, instruments, and experimental set-ups. Lastly, some basic considerations regarding laser safety are described.

Plants have a variety of autofluorescent molecules, giving them characteristic fluorescent peaks when excited. When excited with UV-light, these characteristic peaks occur at approximately 460 nm, 525 nm, 685 nm and 740 nm (Zhao et al., 2020). These peaks can be attributed to pigments, like anthocyanin at 460 nm or carotenoids at 525 nm. However, for these pigments, the characteristic peaks can be variable per plant species, and are dependent on deep UV excitation (Donaldson, 2020).
The two characteristic peaks in the red (685 nm) and the far-red (740 nm) are related to the chlorophyll content of the plant, also referred to as chlorophyll fluorescence (ChlF). Here, the fluorescence emission around 685 nm is associated with Photosystem II (PSII), and the fluorescence emission around 740 nm is associated with Photosystem I (PSI) (Donaldson, 2020).

Measuring ChlF is based on the mechanisms of energy transfer in photosynthesis. The energy absorbed from photons follow a path through one of three ways: 1) the energy is quenched through pigments and the photosynthetic system, referred to as photochemical quenching; 2) the energy is dissipated as heat, called non-photochemical quenching, or 3) the energy is emitted as a photon, referred to as fluorescence (Figure 2.1) (Arief et al., 2023; Chappelle et al., 1984; Pérez-Bueno et al., 2019). The process on energy dissipation between the three processes means that changes in one process, like photochemical quenching, leads to changes in the two other processes (Cendrero-Mateo et al., 2016).

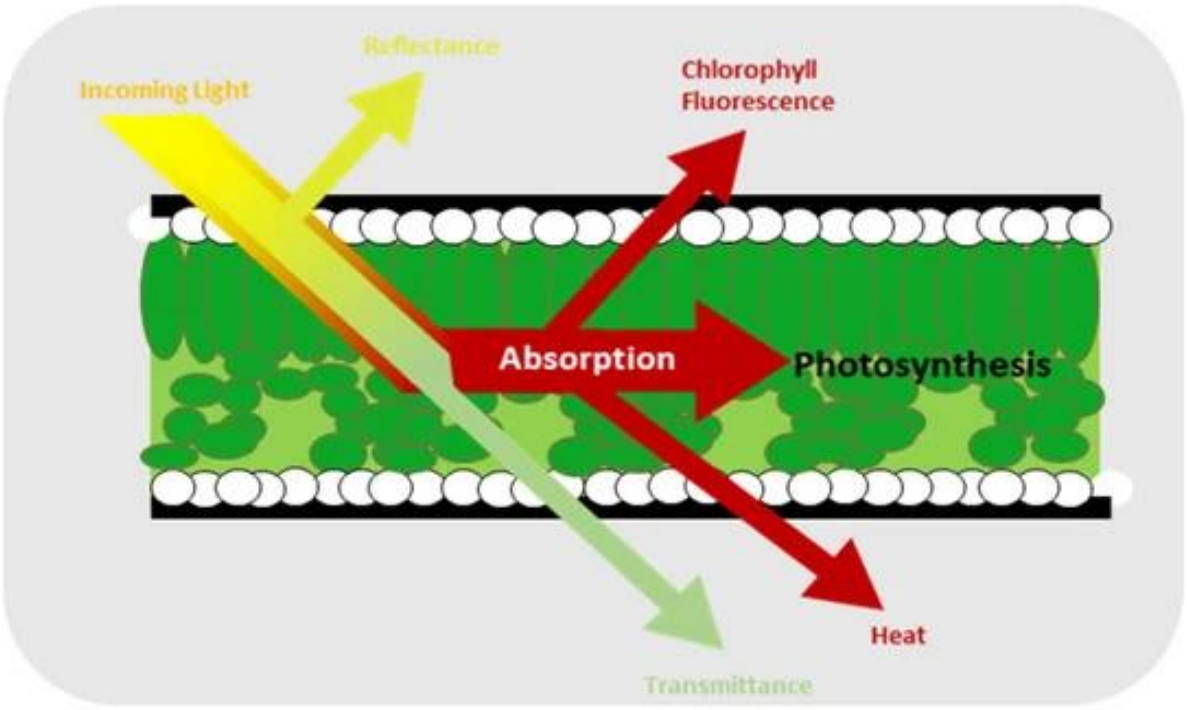

Figure 2.1: The three paths of absorbed light in vegetation: photosynthesis (photochemical quenching), heat (non-photochemical quenching, and chlorophyll fluorescence. Figure derived from Arief et al. (2023)

Because of the direct association of the 685 nm and 740 nm ChlF peaks with photosynthesis activity and efficiency, ChlF emission is used as a measure to detect changes in vegetation growth and health (Donaldson, 2020; Kharcheva, 2014; Pérez-Bueno et al., 2019). Furthermore, in contrast to anthocyanin and carotenoids, chlorophyll is not only excited by UV, but also by blue (400-500 nm) and green (500-600 nm) light (Donaldson, 2020).

The autofluorescence of vegetation related to chlorophyll is not constant. When a plant is adapted in the dark for at least 20 minutes and then moved to the light, the fluorescence emission rises to a maximum and then gradually decreases to a steady state level. This dynamic is called the Kautsky effect and is used to study potential photosynthetic activity (Lichtenthaler et al., 1986). The maximum fluorescence is also observed when vegetation is not adapted to the dark (Kolber et al., 2005). Both dark- and light adapted maximum and steady state fluorescence emissions are used to quantify various variables related to vegetation health.

In literature, three different groups of parameters are identified. First, ChlF parameters that are used to quantify photosynthetic rate and efficiency. Here, fluorescence values from dark and light adapted leaves are used to calculate parameters such as maximum quantum yield of PSII in dark adapted state, effective quantum yield, non-photochemical quenching and photochemical quenching (for details, see Lichtenthaler et al., 2005). Second, the ratio fluorescence decrease (Rdf) is used to quantify the photosynthetic activity (Lichtenthaler et al., 1986). Finally, the ChlF ratio is used as a measure of leaf chlorophyll concentration. This ratio is based on the red and far-red peaks characteristic for chlorophyll fluorescence (Leufen et al., 2014).

The abovementioned parameters are therefore used to measure photosynthetic efficiency, activity, and chlorophyll content. Statistical tests are used to determine differences between groups, like analysis of variance (ANOVA) (Gameiro et al., 2016; Leufen et al., 2014) or t-tests (M. Pérez-Bueno et al., 2016; Truax et al., 2023), or to detect relationship between parameters (Boussadia et al., 2015; M. Cendrero-Mateo et al., 2016). Furthermore, validation data is often collected using destructive measures to, for example, get a precise measure of water or chlorophyll content (Gameiro et al., 2016).

LIF is explored within existing research as a non-destructive method to assess vegetation health. A variety of plant species and vegetation types are used to explore biotic or abiotic stresses and phenotype characteristics. The types of plants used are, for example, trees (Atherton et al., 2016; Boussadia et al., 2015; Kharcheva, 2014; Lichtenthaler et al., 1986; Wang et al., 2018), crops (Du et al., 2020; Fedotov et al., 2017; Kölbl et al., 2023; Leufen et al., 2014), mosses (Truax et al., 2023), or houseplants (Zhao et al., 2020).

Depending on the aim of the research, the methodology of plant care is approached mainly in two different ways. On one hand, vegetation within reach is used, such as campus trees (Wang et al., 2018), or little info is given about the environmental circumstances in which the vegetation grew. Oftentimes, these researches are focusing more on the way fluorescence information can be captured and combined with 3D point data (Wang et al., 2018; Zhao et al., 2020) or capturing fluorescence from a larger distance, e.g. via a drone platform (Lednev et al., 2022a; Wang et al., 2018). On the other hand, detailed growing conditions are given about vegetation when researches consider fluorescence for biotic or abiotic stress detection (e.g. Gameiro et al., 2016; Kautz et al., 2014; Kölbl et al., 2023; Leufen et al., 2014; Truax et al., 2023), or when values such as nitrogen concentration or chlorophyll content are aimed to be estimated based on fluorescence values (Du et al., 2017; Yang et al., 2018).

The way vegetation fluorescence is acquired differs for various research. The primary distinction can be made between an imaging and a non-imaging approach. The imaging approach is either handheld or lab-based and gives fluorescence images of vegetation (Kautz et al., 2014; M. Pérez-Bueno et al., 2016). Non-imaging is either done by handheld devices such as the PAM or using a laser-based set-up (Barták et al., 2015; Fedotov et al., 2017; Gameiro et al., 2016). However, current research shows approaches to combine imaging and non-imaging techniques to map vegetation fluorescence;

various experiments are done using a combination of LIF and LiDAR to map fluorescence in a 3D space (Wang et al., 2018; Zhao et al., 2020), or map fluorescence in 2D, using ground-based or drone platforms (Kölbl et al., 2023; Lednev et al., 2022a).

Using laser as excitation source requires safety-precautions and safety measures to consider, especially when applying LIF measurements in a real-world scenario. Three laser hazard variables to consider are maximum permissible exposure (MPE), intrabeam nominal ocular hazard distance (NOHD) and diffuse nominal hazard zone (NHZ). The MPE is based on power density and exposure time and is different for lasers of various wavelengths. The value tells the maximum power density (in W/cm^2 for continuous laser, J/cm^2 for pulse lasers) that can hit the eye without doing damage for a certain exposure time. The intrabeam NOHD is the distance from which one can look safely directly into the laser and is dependent on the divergence of the laser. Lastly, the diffuse NHZ related to the distance in meters where diffuse reflection (based on a reflectivity of 100% and a viewing angle of 0 degrees) to the eye is safe (Barat, 2019). However, it is important to note that the values for the three mentioned laser hazard variable are given for the worst case, so a lower MPE and larger NOHD and NHZ distances are preferred to ensure safe laser handling.

3. Methodology

Based on the literature review, different experiments are designed to collect data and answer the research questions 2-4 accordingly. To do this, the research following the literature review was divided into three parts, where each part relates to a specific topic within this research. The parts and their related research questions are shown in Figure 3.1.

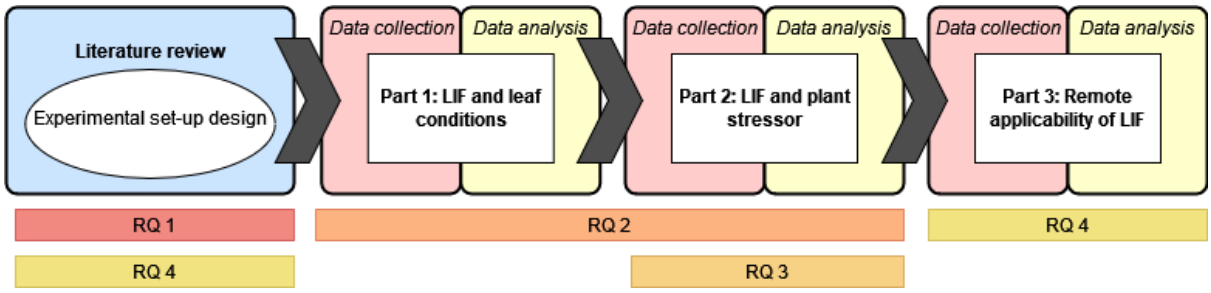

Figure 3.1: Methodology approach taken in this research. The research is divided into four parts; first a literature review, followed by specific experimental part 1, 2, and 3. The corresponding research questions to each part are depicted below the flowchart.

In this chapter, the general approach and the specific methods for each research part are presented regarding data collection, data processing and data analysis, respectively.

3.1. Data collection

Data collection was done in the Optics Lab of the Phenomea building, research facility for postharvest research and agro-food robotics of Wageningen University. In the lab, three continuous-wave laser sources were available to use as excitation source during the experiments. These laser sources emit at a wavelength of 405 nm, 450 nm, and 650 nm. As discussed in the literature review, the power density is an important aspect to consider regarding laser safety whilst still sensing a clear signal, especially since the aim is to assess the applicability of the set-up in a real-world scenario. The intensity profile of 405 nm and 650 nm laser sources were line-shaped, while for 450 nm laser it was dot-shaped. In any case the intensity profile had a Gaussian distribution along the beam axes. Using a focal lens in front of the laser, it was relatively easier to manipulate the size of the laser beam spot for the 405 nm laser. Since the beam spot area was straightforward to calculate, the choice was made to continue the experiments with the 405 nm laser. The experiments presented thus have a laser excitation source of 405 nm, unless stated otherwise.

A schematic overview of the set-up is shown in Figure 3.2. Here, a pyroelectric detector (S405C with PM100D of Thorlabs, USA) was used to measure the average laser power. The emitted fluorescence was recorded by a general-purpose spectrometer, having a 10 µm entrance slit and a grating of 821 lines/mm blazed at 450 nm (OCEAN-HDX-VIS-NIR of Ocean Insight, USA). The fluorescence light is collected by a Φ 2” 180 mm achromatic lens (AC508-180-AB-ML of Thorlabs, USA) in combination with a 10 mm collimating lens (74-VIS of Ocean Insight, USA) screwed onto a SMA-terminated 1000 µm optical fibre (QP1000-2-UV-BX of Ocean Insight, USA). The samples were also imaged using CCD camera (Marlin F145C2 of Allied Vision Technologies, Germany), equipped with a 50 mm lens (VS-5026VM of VS Technology, Japan).

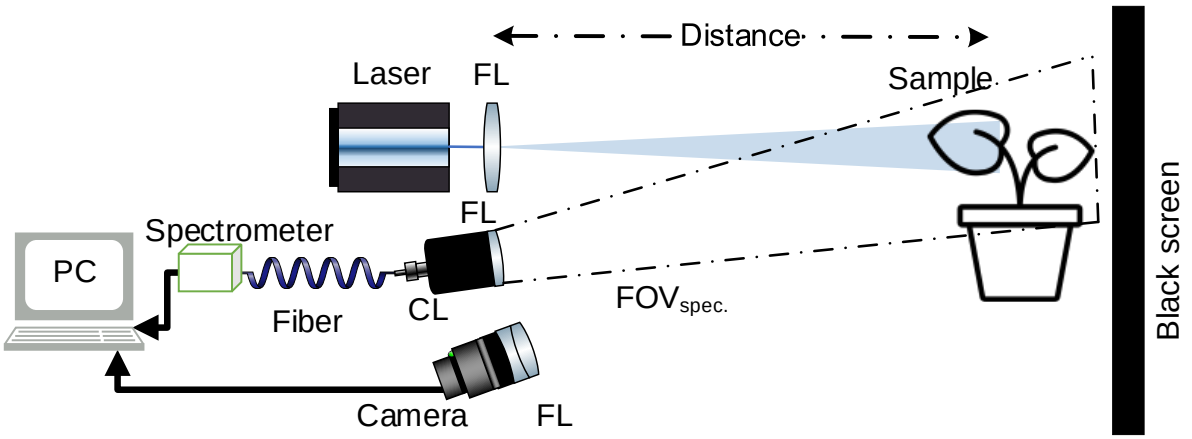

Figure 3.2: Schematic overview of the set-up as used in this research. FL: focal lens; CL: collimating lens; FOV: field of view. The laser source is a low power laser of 405 nm. The distance between the laser, lens and sample is variable. Measurements are stored on a personal computer (PC). The camera is used to see the positioning of the laser beam spot and adjust it if needed.

Data acquisition is done using the software OceanView version 2.0 spectroscopy software of Ocean Insight Inc., USA. Data processing is done in RStudio, using the hyperSpec package (Beleites & Sergo, n.d.).

Various plants were acquired to use during the experiments. The houseplants (Figure 3.3) were bought at garden centre "de Oude Tol", Wageningen on November 20, 2023, and the *violas* (Figure 3.4) were bought at garden centre "Welkoop", Wageningen on February 16, 2024.

From November to December, plants were kept in the thesis room in Gaia, Wageningen Campus. From December to March the plants were kept in the flower room in Phenomea, Wageningen Campus.

Figure 3.3: Canopy pictures of houseplants used in this research: 1) *Pilea* peperomioides; 2) *Coffea* Arabica; 3) *Calathea* leopardine; 4) *Iresine* herbstii "Rich Redstar".

Figure 3.4: Canopy picture of the 6 *violas* used in this research.

Alongside the LIF measurements, SPAD measurements were also taken using the Minolta SPAD. This instrument measures relative chlorophyll content of a leaf using the transmittance of red and infrared radiation (Uddling et al., 2007). As this gives a measurement of relative greenness of plants, the values can be used to compare resulting LIF values. This way, the ability of LIF to detect stress earlier than greenness indices can be assessed as well.

For every part in this research, a short description of the experiments and their aim is given. An overview of all experiments can be found in Appendix A.

3.1.1. Part 1: Leaf conditions and characteristics

The aim of Part 1 in this research was to explore the LIF signal of various plants and compare different parameters that are often used in research to quantify LIF measurements. Furthermore, the results can be used to compare to literature, and to validate the set-up that was designed for this research.

Experiment A: LIF of different species

In this experiment LIF measurements were obtained for every plant as presented in Figure 3.3 and Figure 3.4. This was done in vivo, where one leaf was picked to excite and get the SPAD measurement from. The measurements were taken from a distance of 70 cm, with a power of 157 mW and a beam diameter of 1 cm, giving a power density of 200 mW/cm^2.

Experiment B: Exciting old/young leaves + upper/lower part of the leaf.

Various sources explore the difference in chlorophyll fluorescence (ChlF) between mature and young leaves, as well as the ChlF of the upper and lower of the leaf (Gameiro et al., 2016; Lichtenthaler et al., 1986). Furthermore, a distinction between maximum fluorescence and steady state fluorescence is made (Hsiao et al., 2010; Kolber et al., 2005). In this experiment, a mature and a young leaf were plucked from the *coffea arabica* and the *viola.* To capture the maximum fluorescence (F_m) and the steady state fluorescence (F_s), the data every 1.5 seconds for 4 minutes, as Lichtenthaler et al. (1986) states that F_s is reached after 4 minutes of excitation. To make sure the F_m was captured, the measurement was started

before exciting the leaf. The measurements were taken from 80 cm with a power of 164 mW and a beam diameter of 12 mm, giving a power density of 145 mW/cm^2.

3.1.2. Part 2: Water stress

Part 2 focusses on the use of LIF measurements to detect stress in vegetation. In this research, drought was used as stressor. As water stress affects photosynthetic performance, LIF is expected to capture differences in stressed and not stressed plant earlier than greenness indices (Gameiro et al., 2016). Therefore, two experiments were conducted related to water stress in vegetation, based on Gameiro et al. (2016), pertaining two different ways of inducing water stress.

Experiment C: Fast stress

The fast stress experiment refers to the dehydration of detached leaves. Here, three leaves of *viola* (plant no. 6 in Figure 3.4) were detached and left to dry at room temperature (20 °C). Every hour, LIF and SPAD measurements were taken, with a total of 8 time points. The water content of the leaves is determined by weighing the leaves a every time point and dividing the current weight by the initial weight (Gameiro et al., 2016).

Experiment D: Slow stress

The slow stress experiment refers to the withholding of water to plants for 2 weeks. For this experiment, *viola* no. 1 and no. 2 (as indicated in Figure 3.4) acted as control group, and *viola* no. 3 and no. 4 were withheld from water. The water content of the plants was determined based on the weight of the entire plant (including pot and soil). It is assumed that any weight gain due to plant growth for the duration of the experiment is negligible. All plants were watered to a starting water content – determined as a total weight of 200 grams. The plants were weighted on a daily basis, and the control group was watered up until 200 grams daily.

Every day (except for the weekend due to lab access), LIF measurements and SPAD measurements were taken on a leaf level and on canopy level. On leaf level, the same leaf was measured with LIF using a beam diameter of 15 mm with a power ranging from of 80±2 mW, with a power density of ~45 mW/cm^2. For SPAD, 10 measurements were taken on the same leaf. For the canopy level, the LIF was measured using a beam diameter of 40 mm with the power ranging from of 80±2 mW, with a power density of ~6.4 mW/cm^2. For the SPAD canopy measurement, 10 non-destructive measurements of 10 randomly picked leaves were taken.

3.1.3. Part 3: Remote applicability

The aim of the third part of the research is to assess the applicability of the set-up when measuring at a remote distance. The first variable is the distance between the set-up and the sample. Applying in a real-world scenario, e.g. a greenhouse or agricultural field, measuring would be done a bigger distance than that is usually done for LIF measurements. The second variable that is considered is power density. This variable is of importance when considering laser safety.

Experiment E: Distance

In this experiment the 450 nm laser was used. This laser is a point laser, so the power density was not considered. The *pilea* was used in this experiment, and for the data collection two different approaches were taken. First, a leaf of the *pilea* was excited with 29 mW and the fluorescence excitation was recorded at different distances. For the second approach, the *pilea* was used as well. Here, the fluorescence signal was kept at the same intensity, while changing the laser power and the measuring distance.

Experiment F: Power density

For this experiment the *pilea* was used. Measurements were taken from a distance of 80 cm. The fluorescence signal was recorded with different laser powers and beam diameters. The diameter of the beam was manipulated using a lens in front of the laser and were noted down to later calculate the power density:

$$Power\ density = \frac{Power}{Beam\ area}$$

Equation 1

Where the beam area was calculated as:

$$Beam\ area = \pi * \left(\frac{diameter}{2}\right)^2$$

Equation 2

The diameter was recorded in millimetre (mm) and was multiplied by factor 0.1 before plugged in to Equation 2. The power density is given in mW/cm^2.

3.2. Data processing

Data processing was done in RStudio (4.3.1) using the *hyperSpec* (0.100.0) R package (Beleites & Sergo, n.d.). A description of the research data folder can be found through Appendix A.

Data was read in as hyperSpec object. First a background correction on the data was done. It should be noted that in this research, a suboptimal background correction is done, where the spectrum of only the laser is subtracted from the raw spectra, instead of the spectra of no laser with plant (Lednev et al., 2022a; Lednev et al., 2022b). Still, as the research mainly focusses on relative fluorescence instead of absolute fluorescence values, it is expected that the suboptimal background correction does not influence the results drastically.

After the background correction, the spectra of the desired states are selected. In case of F_m, the maximum spectrum is obtained. In case of F_s, the last 10 recorded spectra are selected and averaged. After that, the spectra are smoothed. Here, Savitzky-Golay smoothing is used as this is widely used to de-noise spectral data (Bian, 2022; Kölbl et al., 2023). Furthermore, if normalization is required, min-max normalization is applied (Gameiro et al., 2016).

3.3. Data analysis

3.3.1. Part 1: Leaf conditions and characteristics

The aim of experiment A was to compare the differences in LIF between different species. Here, spectra were visualised to assess the spectral behaviours. Next to that, the fluorescence ratio FR_{max} was calculated for each species (Equation 3). The mean and standard deviation were noted for both FR_{max} and the SPAD values and visualized in a scatter plot. The Pearson correlation was calculated to assess if there is a relationship between the FR_{max} and SPAD. Lastly, a linear model was fitted with SPAD as predictor variable and FR_{max} as response variable, tested again a significance value of 0.05.

As part of validation of the set-up, a visual comparison is made between results from experiment B and from Gameiro et al. (2016) and Lichtenthaler et al. (1986). To do this, the data from experiment B was normalized and visualized.

Next to that, the data resulting from experiment B is used to explore several parameters that are used in literature to quantify ChlF. A commonly used parameter to quantify ChlF is the ratio between the red and far-red peak of the steady state fluorescence spectra, calculated as:

$$ChlF\ ratio = \frac{F_{red}}{F_{far-red}}$$

Equation 3

Various combinations of wavelengths are proposed in literature to calculate the ratio, for example, F_{690}/F_{730} (Gameiro et al., 2016), F_{690}/F_{740} (Lichtenthaler et al., 1986), or F_{680}/F_{740} (Pérez-Bueno et al., 2019). As the ratio calculation is related to the ChlF peaks, here the ratio is also calculated using the wavelength where the maxima of the red (680-695 nm) and far-red peaks (725-750 nm) are.

Furthermore, F_m and F_s are also often used to assess vegetation fluorescence and derived parameters are related to photosynthesis activity and efficiency (Lichtenthaler et al., 1986). Here, often a distinction is made between obtaining these values for dark-adapted plants, and light-adapted plants. Values obtained in both situations are often combined to calculate different parameters, such as F_v/F_m (Kolber et al., 2005). In the context of this research, dark adaptation is not possible. However, values obtained in light conditions can still yield usable parameters. Kolber et al. (2005) used pulsed laser to calculate the efficient quantum yield (EQY) during the day. Therefore, the possibility of calculating this parameter using a continuous-wave laser is explored. The EQY is calculated as:

$$EQY = \frac{(F_m - F_s)}{F_m}$$

Equation 4

Where F_m is the maximum fluorescence yield when the laser is turned on, and F_s is the steady state fluorescence, reached after 4 minutes according to Lichtenthaler et al. (1986) (Figure 3.5A)
Next to the EQY, the ratio fluorescence decrease (Rfd) is also a parameter that takes the maximum and steady state fluorescence to quantify the potential photosynthetic activity of a leaf (Lichtenthaler et al., 1986), and is calculated as:

$$Rfd\ = \frac{(F_m - F_s)}{F_s}$$

Equation 5

However, considering real-world applications, Hsiao et al. (2010) argue that 4 minute measurements are unrealistic and proposed the Dynamic Fluorescence Index (DFI) as alternative to Rdf or EQY. Here, DFI is defined as the maximum distance between the fluorescence curve at a wavelength and a linear line between F_m and F_e, where F_e is fluorescence intensity measured between 100 seconds and 300 seconds (Figure 3.5B) (Hsiao et al., 2010). As Hsiao et al. (2010) found the most representative DFI at F_e = 170 seconds, this timestamp was used in this research. Furthermore, the EQY, Rfd and DFI are calculated at 690 nm, 720 nm, and 740 nm, representing the red peak, the dip between the two peaks, and the far-red peak, respectively. The relationship between the parameters is assessed using Pearsons's correlation.

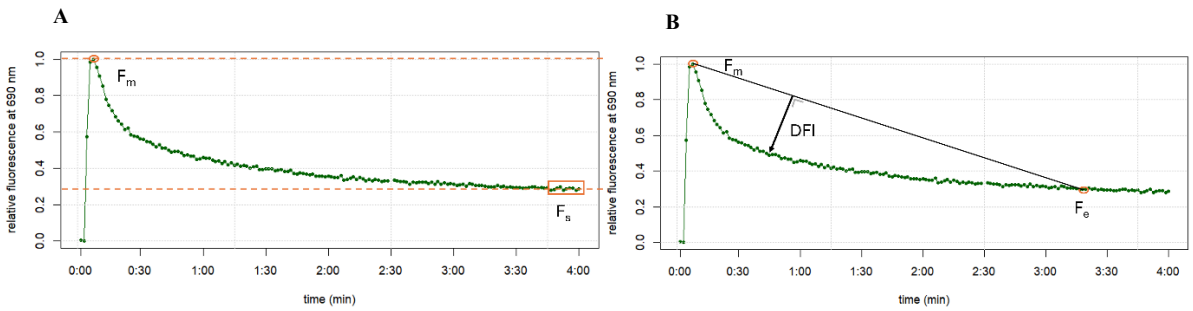

Figure 3.5: A) Fluorescence values measured for 4 minutes, capturing the Fm and Fs. B) Determination of the DFI as proposed by Hsiao et al. (2010). Spectra retrieved from experiment B, mature *viola* leaf, upper side.

3.3.2. Part 2: Water stress

Part two of the research aims to assess the effect of water stress on the LIF signal of plants. The design of the stress experiment is based on Gameiro et al. (2016), and divided into two stresses, referred to as "fast stress" and "slow stress". The results are based on the steady state fluorescence spectra and are normalized, as done by Gameiro et al. (2016).

Fast stress

The spectra of the three detached leaves (A, B, and C) were visualised for each recorded timepoint. After that, the F_{690}/F_{730} ratio was plotted against the water content (H%), and the relationship between the two variables were explored using Pearsons' correlation and by fitting a linear regression for every leaf. Furthermore, SPAD values that were recorded over the day were visualized in a boxplot and using a t-test, the SPAD values at hour 0 (h0) and hour 7 (h7) were tested against a significance value of 0.05 to see whether there is a significant difference in SPAD values between the two time-points.

Slow stress

For the slow stress experiment, measurements at leaf level and canopy level were recorded on 8 days, between March 5 (day 1) and March 14 (day 10). First, the H% of the control and stress group were plotted over the duration of the experiment. Using linear regression, H% was assessed to see whether there was a significant difference over time. After that, the data was analysed on leaf and canopy level as described in this section.

First, the spectra were visualized for the start of the experiment, followed by an intermediate measurement, and subsequently the end of the experiment, corresponding to day 1, day 4, and day 10, respectively. Next, the F_{690}/F_{730} ratio was compared against time and/or H%. Using Pearsons correlation and linear regression, the relationship between time and/or H% and the F690/F630 ratio was assessed. Finally, SPAD values were obtained for day 1 and day 10. For each *viola* it was assessed whether the SPAD values were significantly different between the two time points.

Lastly, the ratio values on leaf and canopy levels were compared to see whether there is a correlation between canopy and leaf level values.

3.3.3. Part 3: Remote applicability

Distance:

The aim of experiment E was to assess the relationship between distance and the ChlF signal, and how laser power plays a role in that as well. For the first part of the experiment, the laser power stayed consistent. The recorded ChlF spectra were visualised. Next to that, the ChlF relative values were taken at wavelength 690 nm, 720 nm, and 740 nm, and plotted to the different distances, to visualise the type of relationship between ChlF and distance. Based on the inverse squared law, an inverse squared relationship was fitted (Marti-Lopez et al., 2004)

In the second part of the experiment, the ChlF signal intensity was kept consistent whilst adjusting the power and distance. The relationship between power and distance was visualised, and based on visual inspection the relationship was assessed fitting a second-order polynomial regression.

Power density:

The aim of the experiment was to assess the relationship between power density and the measured signal of the ChlF. This was approached in two ways. First, the recorded ChlF at 690 nm, 720 nm and 740 nm were plotted against the power density. Visual assessment suggested a quadratic relationship; hence a second order polynomial regression was fitted.

Next to that, the calculated F_{690}/F_{740} ChlF ratio was plotted against the calculated power density. A visual assessment suggested a quadratic relationship, and thus a second-degree polynomial regression was fitted.

4. Results

4.1. Part 1: Leaf conditions and characteristics

Laser induced fluorescence of different plant species

Figure 4.1 shows the ChlF spectra of the different plant species used in experiment A. The figure shows that each species displays a different characteristic ChlF curve besides the different values in intensity. The *calathea*, *iresine* and *viola 1* show the highest peak around 690 nm, while the *pilea* and *coffea* show their highest peak around 740 nm. Furthermore, the *iresine*, *pilea* and *coffea* clearly show two peaks, while the lower peaks of the *calathea* and *viola* are less distinguishable.

Figure 4.2 shows the ChlF spectra of the six *viola* plants. Here, a difference in relative fluorescence intensity is observed, but the six spectra show similar characteristics within the species, compared to the spectra of the different species in Figure 4.1.

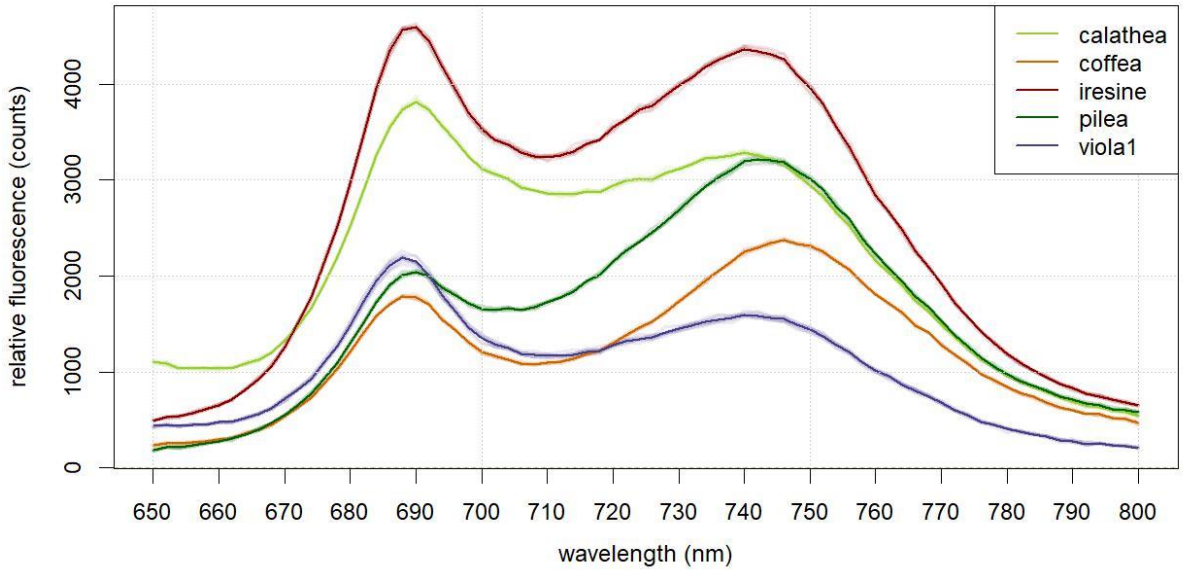

Figure 4.1: Steady state spectra of the chlorophyll fluorescence of the different plant species (excluding *viola* 2-6).

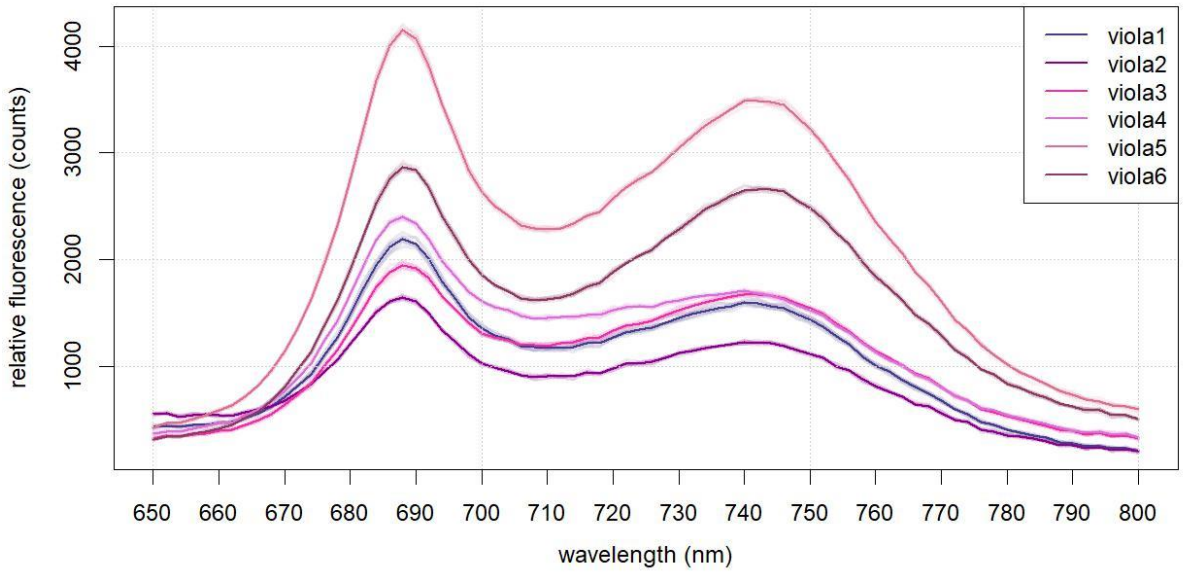

Figure 4.2: Chlorophyll fluorescence spectra of the six *viola* plants.

Next to the ChlF spectra, SPAD values of the excited leaves were recorded. Figure 4.3 shows the recorded SPAD values per species plotted against the ChlF ratio based on the maximum peaks (FR_{max}). For every plant, the mean value to SPAD and FR_{max} is plotted with error bars for both parameters. The plot shows the variation within a plant is higher for the SPAD values than the FR_{max} values. The *coffea* and *pilea* both show high SPAD values and low ratio values, whereas *iresine* and *calathea* show high ratio values and lower SPAD values. The Pearson correlation between the FR_{max} and the SPAD values shows a moderate relationship (r = -0.46). However, the predictive ability using linear regression gives an R-squared of 0.18, with a p-value of $1.6e^{-6}$. The linear regression is significant, but only captured 18% of the variation in the data.

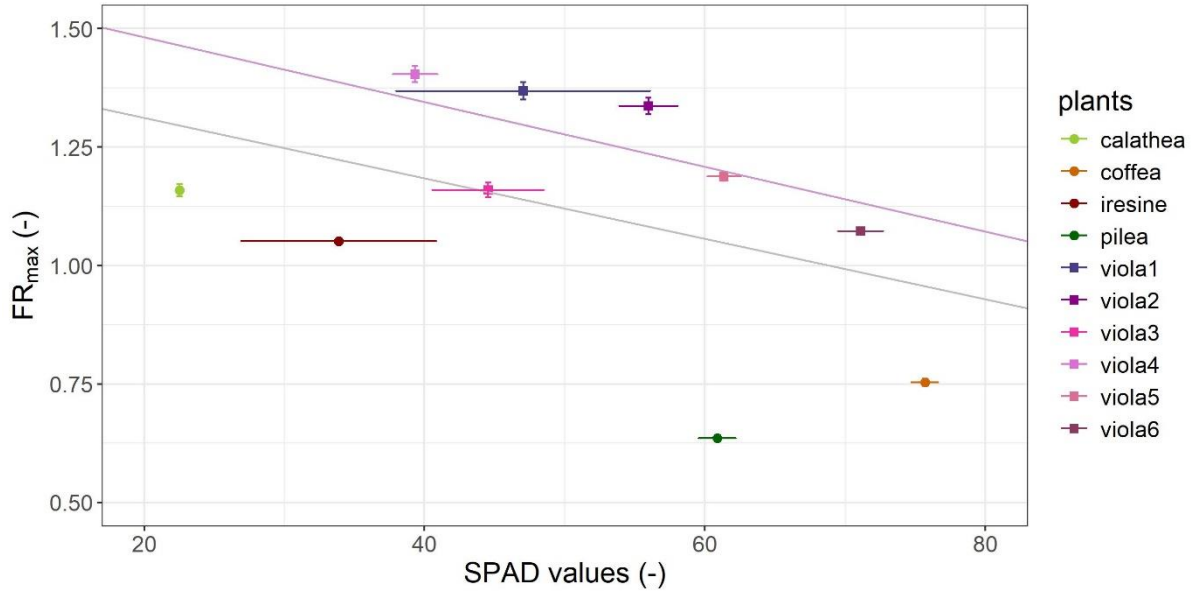

Figure 4.3: Scatterplot of recorded SPAD values and the fluorescence ratio FR_{max}. The grey line denotes the fitted regression line for all species (R-squared = 0.18, p-value = 1.6e-5), the purple line denotes the fitted regression for the *violas* (R-squared = 0.40, p-value = 1.77e-7).

LIF of mature and young leaves + upper and lower side of leaves

The ChlF spectra of a mature and young leaf of a *coffea* and a *viola* are shown in Figure 4.4A and Figure 4.4B, respectively. The young leaf of the *viola* shows a higher fluorescence intensity than the mature leaf; the young leaf of the *viola* shows mainly a higher fluorescence intensity between the fluorescence peaks, and only slightly higher values at the peaks.

Figure 4.4C and Figure 4.4D show the ChlF of the lower and upper part of a mature leaf of *coffea* (3.4C) and *viola* (3.4D). The spectra of the *coffea* shows a clear difference in spectral behaviour: the lower part of the leaf has a higher fluorescence intensity and is the spectral peak around 690 nm higher than the peak around 740 nm. The ChlF of the upper part of the leaf shows a higher peak at 740 nm. The *viola* leaf shows a big difference in fluorescence intensity between the upper and lower part of the leaf. Here, the lower part of the leaf has a higher fluorescence intensity compared to the upper part. Furthermore, the peaks are much more pronounced for the lower part of the leaf than for the upper part of the leaf.

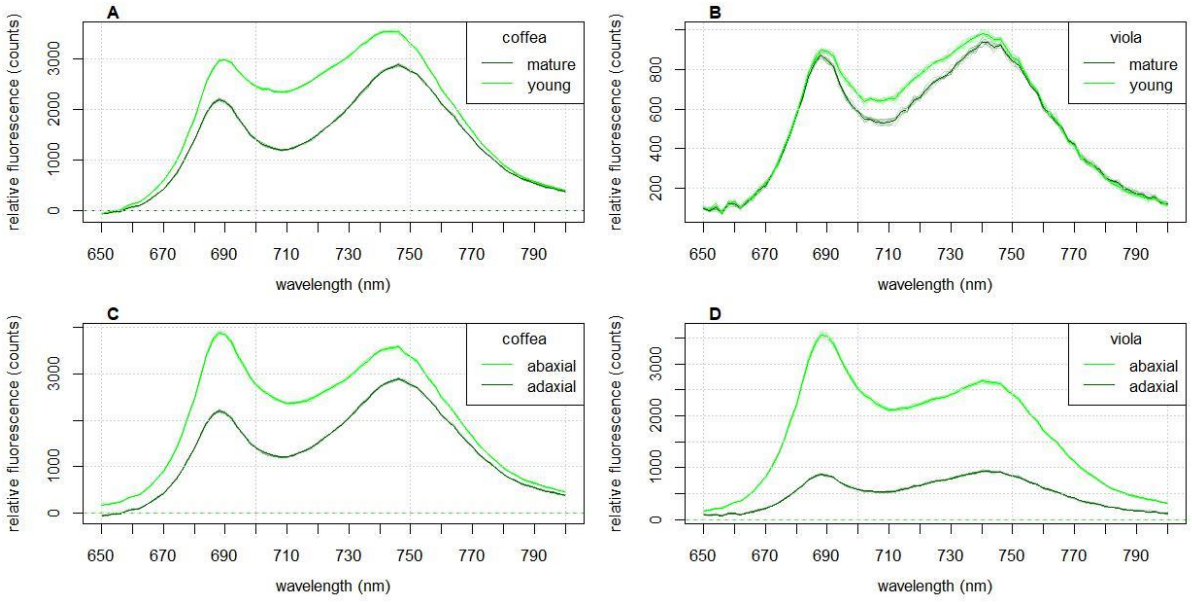

Figure 4.4: A) Spectra of mature and young leaf (upper side) of *coffea*; B) Spectra of mature and young leaf (upper side) of *viola*; C) Spectra of upper and lower side of mature *coffea* leaf; D) Spectra of upper and lower side of mature *viola* leaf.

Exploring ChlF parameters

The data collected for experiment B is used to explore various ChlF parameters, namely peak ratios, Rfd, EQY, and DFI.

As mentioned in the methodology, various peak ratios are used in literature. For this research, three combinations are selected and compared. These are the F_{690}/F_{730} ratio, the F_{690}/F_{740} ratio, and the FR_{max}. The values for the different ratio's found for the spectra are presented in Table 4.1. Here, the F_s as well as F_s are considered. The results show that F_m has a higher value for all three ratios compared to F_s. Furthermore, the mature leaves show lower ratio values compared to the young leaves, and the adaxial side of the leaf shows lower ratio values compared to the abaxial side. The three different ratios have a strong relationship, where FR_{max} and F_{690}/F_{740} have the highest correlation ($r = 0.999$), and FR_{max} and F_{690}/F_{730} has the lowest correlation ($r = 0.965$) (Appendix B, Table B.0.1).

Table 4.1: Different ratio values for steady state (Fs) and saturating fluorescence spectra (Fm). Conditional formatting is used where a gradient from red-yellow-green highlights low to high ratio values. The side of the leaves is denoted by "ab" (abaxial) or "ad" (adaxial).

			F_s			F_m		
plant	**age**	**side**	**FR_{max}**	**F_{690}/F_{730}**	**F_{690}/F_{740}**	**FR_{max}**	**F_{690}/F_{730}**	**F_{690}/F_{740}**
coffea	mature	ab	1.08	1.31	1.1	1.54	1.84	1.53
		ad	0.76	1.05	0.79	1.03	1.48	1.07
	young	ab	1.37	1.55	1.37	1.71	1.95	1.7
		ad	0.84	0.98	0.85	1.01	1.23	1.03
viola	mature	ab	1.33	1.46	1.33	1.74	1.91	1.71
		ad	0.93	1.07	0.91	1.44	1.72	1.41
	young	ab	1.48	1.56	1.46	1.88	2.06	1.84
		ad	0.91	1.01	0.91	1.44	1.64	1.41

Furthermore, a comparison is made between the ratio's calculated from LIFT spectra and steady state spectra (Figure 4.5).

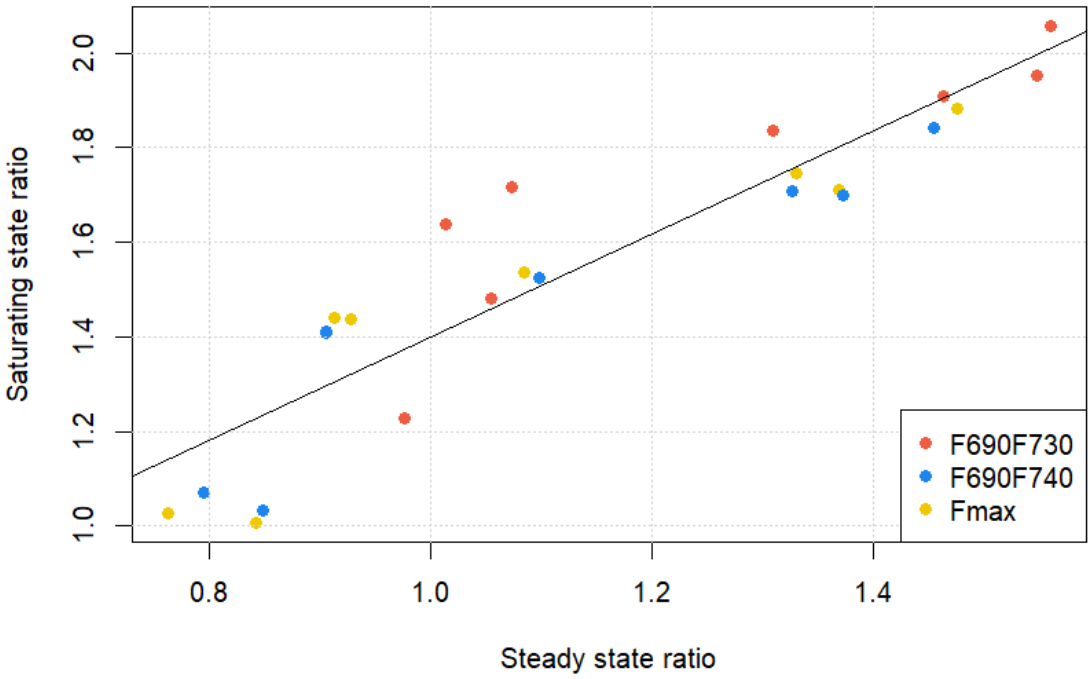

Figure 4.5: Scatterplot of calculated fluorescence ratios for Fs and Fm. Linear line shows the fitted linear regression line, based on the spectra retrieved from the *viola* and *coffea* values presented in Figure 4.4.

The calculated ratios between the steady state ratios and the saturating state ratios presented in Figure 4.5 show a strong relationship (r = 0.92). The linear regression model with steady state ratio as predictor variable and saturating state as response variable shows a significant adjusted R^2 value of 0.84 (p-value = $2.2e^{-10}$).

Looking at the correlation between F_s and F_m per ratio, the FR_{max} and F_{690}/F_{740} both show a correlation of r = 0.93, while F_{690}/F_{730} shows r = 0.88. Furthermore, the F_s shows a strong predictability for F_m for both FR_{max} and F_{690}/F_{740}, with an adjusted R^2 of 0.84 (p-value < 0.05).

Other parameters that were selected are the EQY, Rfd, and DFI. The values of these parameters are shown in Table 4.2.

Table 4.2: Resulting values for EQY, Rfd, and DFI for wavelength 690 nm, 720 nm, and 740 nm. Conditional formatting is applied per wavelength, where a gradient from red-yellow-green highlights low to high values. The side of the leaves is denoted by "ab" (abaxial) or "ad" (adaxial).

			690 nm				**720nm**				**740 nm**		
plant	**age**	**side**	***EQY***	***Rfd***	***DFI***		***EQY***	***Rfd***	***DFI***		***EQY***	***Rfd***	***DFI***
coffea	mature	ab	0.63	1.67	0.56		0.49	0.98	0.5		0.5	0.99	0.5
		ad	0.71	2.48	0.6		0.59	1.45	0.53		0.62	1.64	0.55
	young	ab	0.65	1.9	0.62		0.56	1.28	0.57		0.58	1.38	0.59
		ad	0.61	1.54	0.61		0.51	1.03	0.57		0.52	1.07	0.56
viola	mature	ab	0.79	3.71	0.6		0.73	2.64	0.55		0.73	2.7	0.56
		ad	0.84	5.16	0.69		0.74	2.82	0.64		0.76	3.14	0.67
	young	ab	0.81	4.16	0.67		0.74	2.84	0.62		0.76	3.09	0.63
		ad	0.85	5.81	0.73		0.77	3.32	0.7		0.77	3.31	0.7

The EQY and DFI values show somewhat similar values for the *coffea* in all wavelengths, while the EQY shows a higher value for the *viola* compared to the DFI. The Rfd shows a higher value compared to the other two parameters, where the Rfd values for the *viola* at the three selected wavelengths are higher than for the *coffea*. Furthermore, the EQY and DFI to not show much difference between the adaxial or abaxial side or between the mature and young leaf. Rdf shows different values between leaf side and age.

All three parameters show a high correlation within the parameter between the different wavelengths ($r > 0.96$). DFI shows overall a higher correlation with Rfd ($r > 0.8$) compared to EQY ($r < 0.8$). The overall correlation values are the highest between Rfd and EQY ($r > 0.9$) (Appendix B, Table B.0.2).

Assessing the relationship between the ChlF ratios and the photosynthesis parameters (Appendix B, Table B.0.3), the Pearson correlation between the F_s ratios and the photosynthesis parameters is very low, ranging between -0.26 and 0.22. The F_m ratios show a low correlation with the DFI (between 0.015 and 0.19) and shows a low to moderate positive relationship with EQY and Rdf values (between 0.23 and 0.44).

4.2. Part 2: Water stress

Fast stress

The fast stress experiment aims to capture the changing ChlF of detached *viola* leaves. The three leaves, A, B, and C (Appendix C, Figure C.0.1), were measured every hour, for eight hours, denoted as h0 (hour zero) until h7 (hour 7). The ChlF spectra of every leaf recorded over time is shown in Figure 4.6.

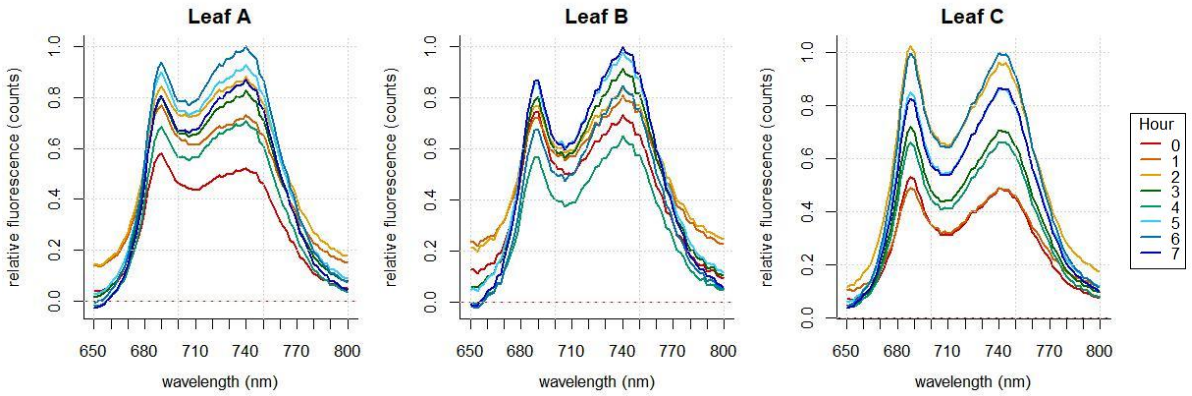

Figure 4.6: Spectra recorded in the fast stress experiment for every hour for leaf A, leaf B, and leaf C.

The spectra show different overall ChlF behaviour between the three leaves. Leaf A has a less pronounced peak in the far-red spectrum compared to leaf B and C. Between leaf B and C, the spectra show a difference in peak height – the spectra of leaf C show somewhat similar height in the peak regardless of time, while the spectra of leaf B show a difference in relative height between the red and far-red peak at the same time-point.

Comparing the spectra of the leaves over time, all three leaves show a higher relative fluorescence at h7 compared to h0. However, the fluorescence does not increase over time. For example, the spectra of leaf A show that h1 and h2 yield higher values than h3, with h2 also yielding higher values compared to h4 and h7. For leaf B, h0 yield a higher value than h4, and h6 yields lower values compared to the other hours except for h4 in the red peak region. Leaf C show a higher h2 yield compared to the other spectra, and h6 shows a higher emission than h7.

Figure 4.7 shows the linear relationship of each leaf with water content (H%) and the ChlF ratio F_{690}/F_{730}.

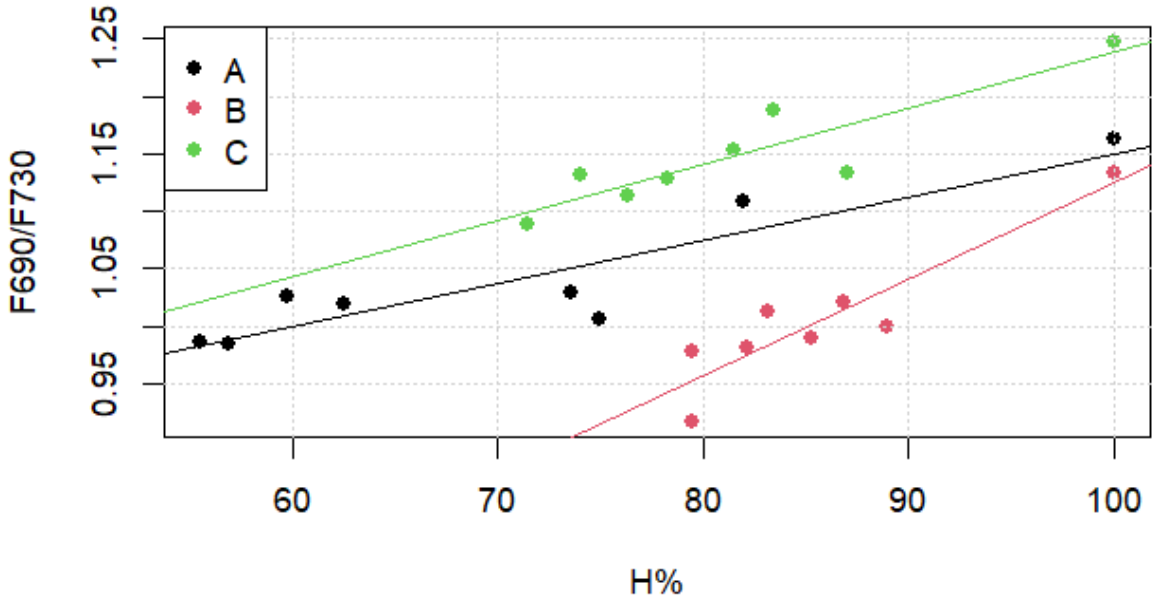

Figure 4.7: Scatterplot of H% and F_{690}/F_{730} for every leaf. Lines denote the fitted linear regression line for every leaf.

Every leaf shows a high correlation ($r > 0.89$) between H% and F_{690}/F_{730} and a significant linear regression between the two variables (Adjusted $R^2 > 0.77$; p-values < 0.05) (Appendix D, Table D.0.1).

Finally, SPAD values of the leaves were recorded for each hour (Figure 4.8). Between the first and last SPAD measurement, no significant difference was found.

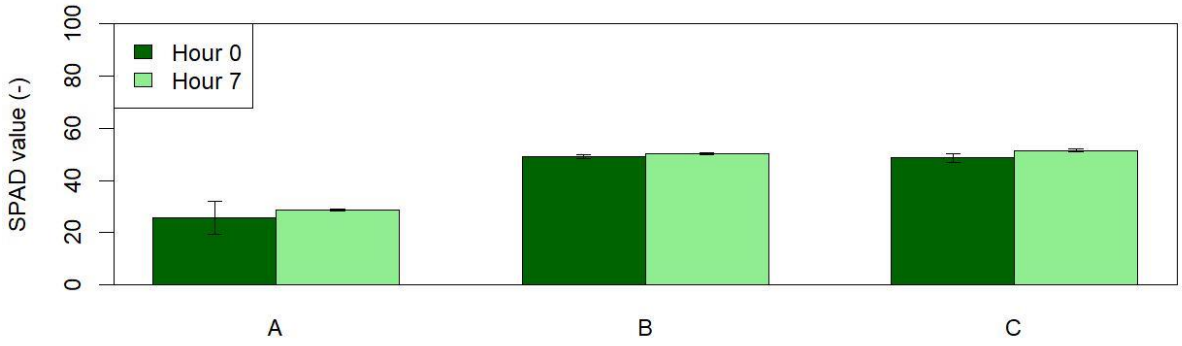

Figure 4.8: SPAD values compared for h0 and h7 for leaf A, leaf B, and leaf C. The error bars show one standard deviation. No significant difference was found in SPAD values between h0 and h7 for each leaf.

Slow stress

During the slow stress experiment, measurements were collected on leaf level and canopy level. The water content of the control group and the stress group was recorded over the duration of the experiment (Appendix D, Figure D.0.1). For the control group, no significance was found for a change in water content over time (p-value = 0.345, R^2 = -0.003), which was expected as the control group was still watered. For the stressed group, the decrease of water content over time is significant (p-value = 1.81e-11, R^2 = 0.961).

In this section, first the results of the leaf level are presented, followed by the results of the canopy level. Before and after picture of the excited leaves and from the canopies can be found in Appendix C, Figure C.0.2 and Figure C.0.3, respectively.

Leaf level

Figure 4.9 shows the ChlF spectra of the four *violas*, measured at three different dates. *Viola* 1 and *viola* 3 show very similar fluorescence spectra on the three different dates. *Viola* 2 shows similar fluorescence spectra for the first and last date but shows higher relative fluorescence emission for the middle date. Lastly, *viola* 4 shows 3 different fluorescence emission spectra, where the last date has the lowest fluorescence emission, and the first date shows the highest fluorescence emission.

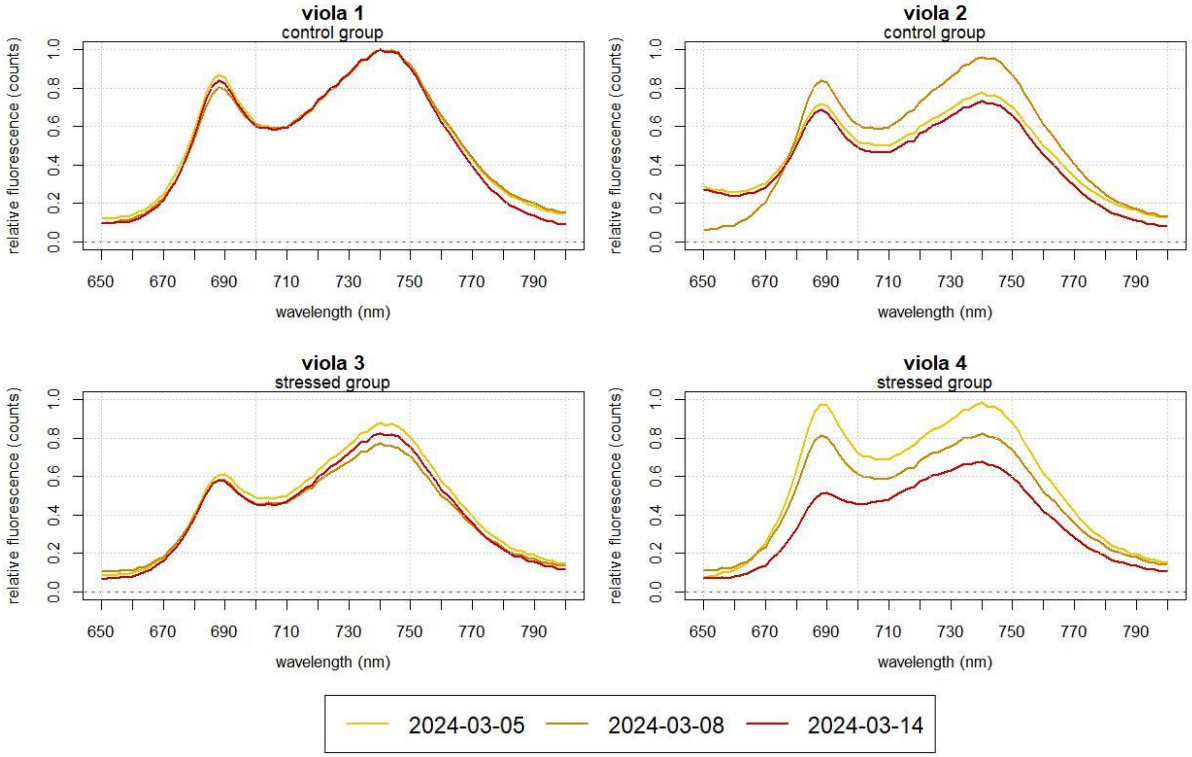

Figure 4.9: Fluorescence spectra of the plants in the slow stress experiment at leaf level, recorded on March 5, March 8, and March 14, at leaf level. Here, *violas* 1 and 2 are the control group, and *violas* 3 and 4 are the stressed group.

Both plants from the control group have a mean H% of 90% (*viola* 1, standard deviation (sd) = 4.5%) and 93.1% (*viola* 2, sd = 2.9%). The mean F_{690}/F_{730} values of *viola* 1 and *viola* 2 are 0.95 (sd = 0.07) and 0.99 (sd = 0.05), respectively.

Figure 4.10 shows the F_{690}/F_{730} plotted against H%. *Viola* 3 shows a moderate negative correlation between H% and F_{690}/F_{730} (r = -0.51), *viola* 4 shows a strong positive correlation between H% and F_{690}/F_{730} (r = 0.86). The linear regression fitted for *viola* 3 does not show a significant prediction of F_{690}/F_{730} by H% (R^2 = 0.13, p-value = 0.197). The linear regression fitted for *viola* 4 does show a significant prediction of F_{690}/F_{730} by H% (R^2 = 0.70, p-value = 0.006). For the control group, no significant difference is found in F_{690}/F_{730} between the first and last day of the experiment (Appendix D, Figure D.0.2)

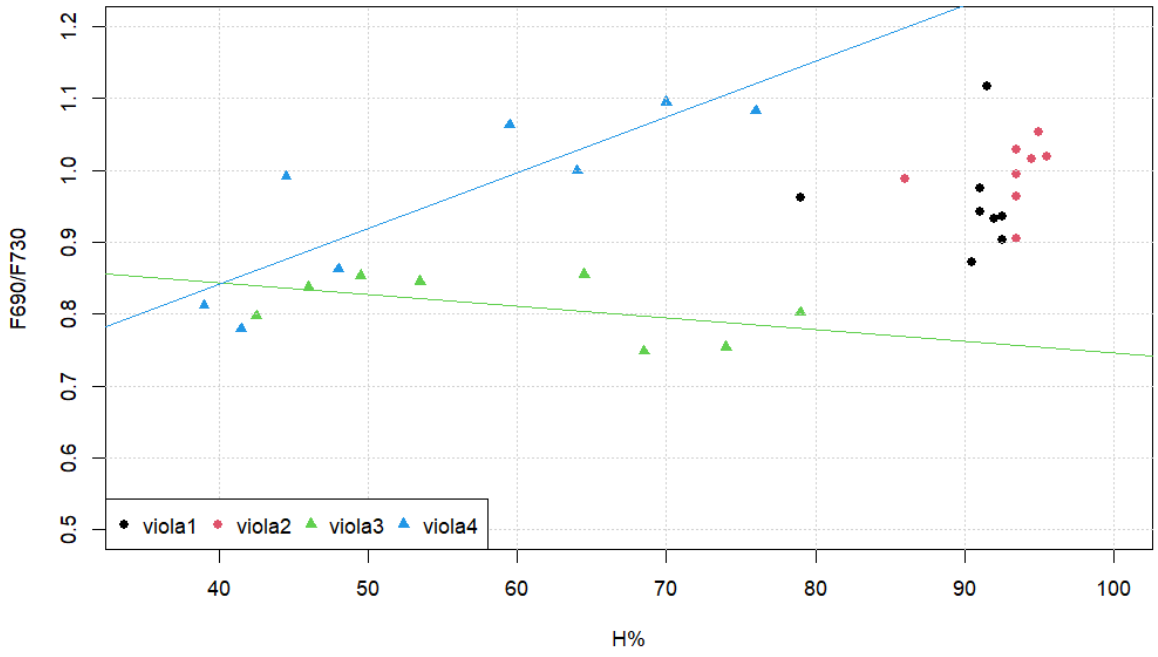

Figure 4.10: Scatterplot of the 4 *violas* recorded H% and F690/730 values. The green line presents the fitted regression line for *viola* 3, and the blue line presents the fitted regression line for *viola* 4.

Figure 4.11 shows the SPAD values recorded of *viola* leaves at the start date and the end date of the stress experiment. Here, the SPAD value for *violas* 1, 2, and 3 show a significant difference in SPAD values, where the mean value is lower at the end of the experiment. For *viola* 4, no significant difference was found.

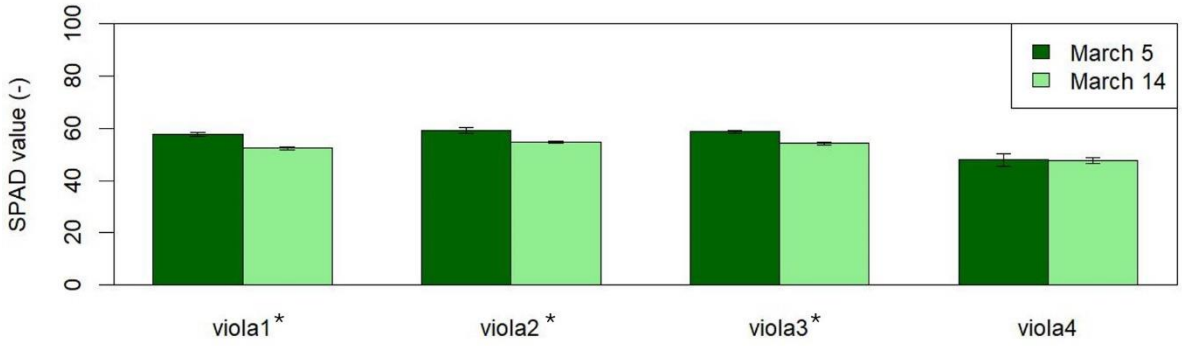

Figure 4.11: Recorded SPAD values on leaf level for the first and last day of the experiment. *Violas* 1, 2, and 3 show a significant difference between the first and last day of the experiment. For *viola* 4, no significant difference was found. The error bars present one standard deviation, significance found in a group is denoted with an asterisk (*).

Canopy level

Figure 4.12 shows the ChlF spectra of the four *violas* on a canopy level. Here, *viola* 1 shows a lower peak in the red and a higher peak in the far red for day 1 compared to the other two days. Day 4 and day 10 show the same ChlF emission. *Viola* 2 has a lower ChlF emission for day 4 compared to day 1, and day 10 shows the highest ChlF emission. For *viola* 3, day 1 has the highest relative fluorescence.

Day 4 and day 10 show the same emission in the far-red peak, but day 10 shows a lower emission in the red peak compared to day 4. For *viola* 4, the ChlF spectra show the same values for day 1 and day 4, and a lower ChlF emission for day 10.

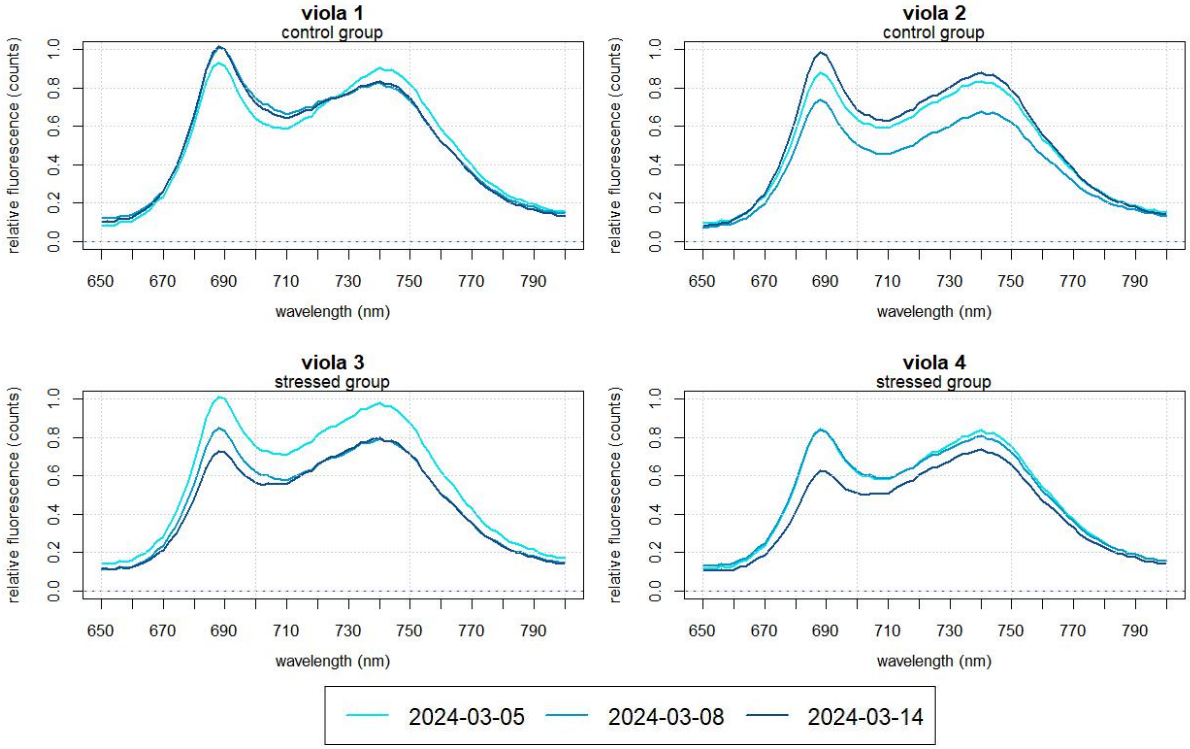

Figure 4.12: Fluorescence spectra of the plants in the slow stress experiment at canopy level, recorded on March 5, March 8, and March 14, at leaf level. Here, *violas* 1 and 2 are the control group, and *violas* 3 and 4 are the stressed group.

Comparing between the first and the last day of the experiment, the ratio is higher on the final day when compared with the ratio value on the first day for both control groups. For *viola* 3 and *viola* 4, the stressed group, the ratio values are lower on the last day compared to the first day. Only for *viola* 4 a significant difference in ratio was found between the first and last experiment day (Appendix D, Figure D.0.3).

The ratio values plotted against the H% (Figure 4.13) shows a strong positive correlation for *viola* 3 ($r = 0.80$) and a strong positive correlation for *viola* 4 ($r = 0.86$). The linear regression fitted for *viola* 3 does not show a significant prediction of F_{690}/F_{730} by H% ($R^2 = 0.13$, p-value = 0.197). The linear regression fitted for *viola* 4 shows a significant prediction of F_{690}/F_{730} by H% ($R^2 = 0.70$, p-value = 0.006).

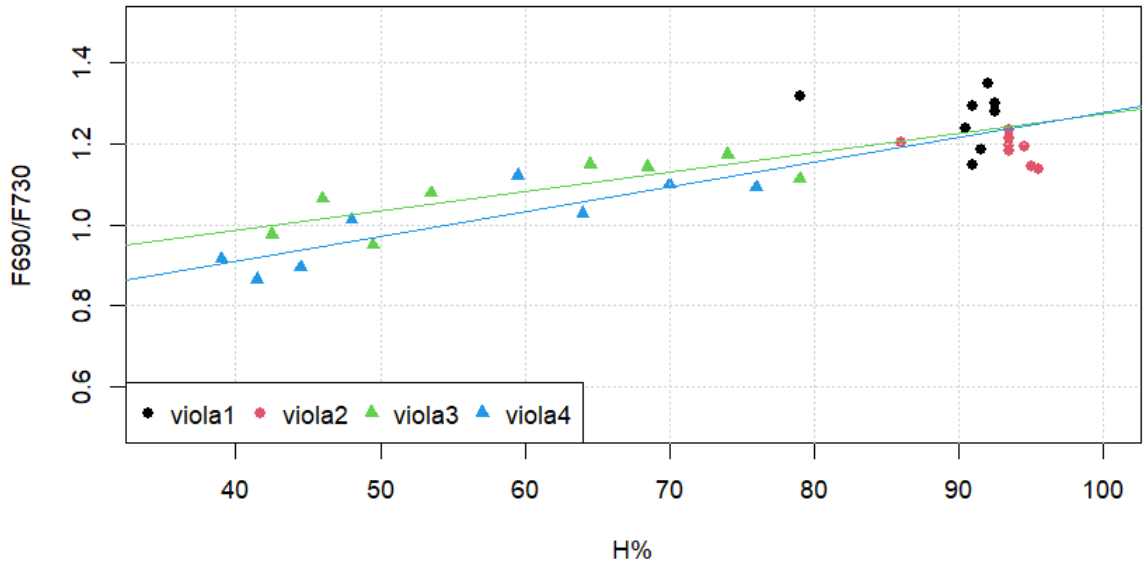

Figure 4.13: Scatterplot of the 4 *violas* recorded H% and F690/730 values. The green line presents the fitted regression line for *viola* 3, and the blue line presents the fitted regression line for *viola* 4.

Figure 4.14 shows the SPAD values recorded of *viola* canopies at the start date and the end date of the stress experiment. Here, the SPAD value for *violas* 1, 2, and 4 show no significant difference in mean SPAD values. For *viola* 4, a significant difference in mean SPAD value was found (p-value = 0.045).

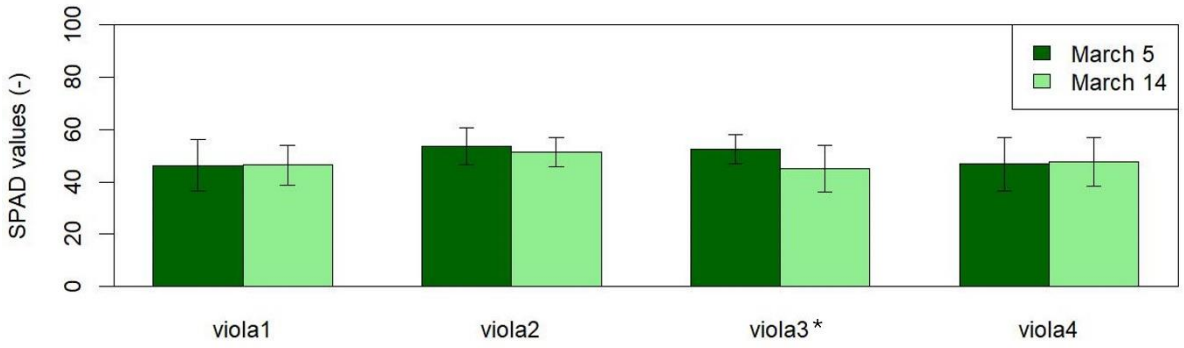

Figure 4.14: Recorded SPAD values on canopy level for the first and last day of the experiment. *Violas* 1, 2, and 4 show no significant difference between the first and last day of the experiment. Only for *viola* 3, a significant difference in mean SPAD value is found. The error bars present one standard deviation, significance found in a group is denoted with an asterisk (*).

Comparison leaf and canopy

The correlation between canopy level and leaf level, considering all the datapoints, is low (r = 0.27). For each plant, *violas* 1, 2, and 3 show a negative correlation of r = -0.48, r = -0.70. and r = -0.45. respectively. *Viola* 4 shows a positive correlation, with r = 0.80 (Appendix D, Figure D.0.4).

4.3. Part 3: Remote applicability

This section presents the results of experiments E and F where the applicability of the set-up was explored in relation to remote measuring. Two variables, distance and power density, were assed, and are discussed respectively.

Distance

Figure 4.15 shows spectra of the *pilea*, acquired with the same laser power (29 mW) at different distances. In the figure, the spectrum taken at a nearby distance (20 cm) has a higher relative fluorescence compared to the measurement taken at 80 cm and 180 cm. The figure shows a decrease in ChlF intensity by an increase in distance.

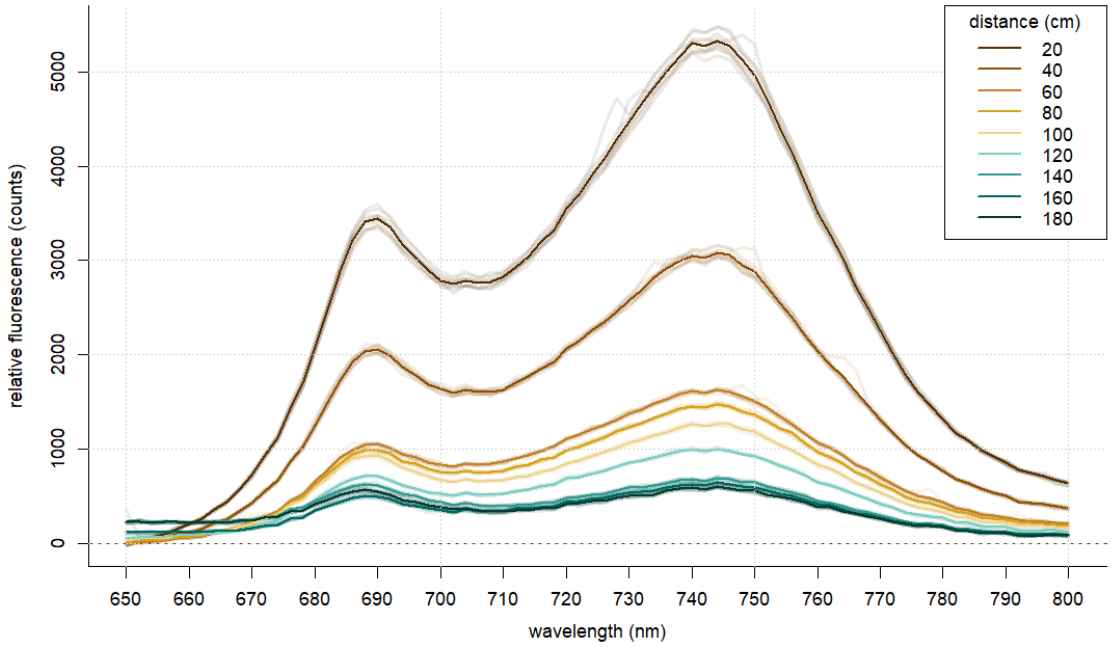

Figure 4.15: ChlF spectra of *pilea* from various distances with an excitation power of 29 mW.

Figure 4.16 shows the fluorescence intensity from Figure 4.15 at 690 nm, 720 nm and 740 nm plotted against the distance. The regression line shows the inversed squared relationship between fluorescence intensity and distance. The fitted relationships show a significant adjusted R-squared value of 0.913, 0.908 and 0.908 for 690 nm, 720 nm, and 740 nm, respectively.

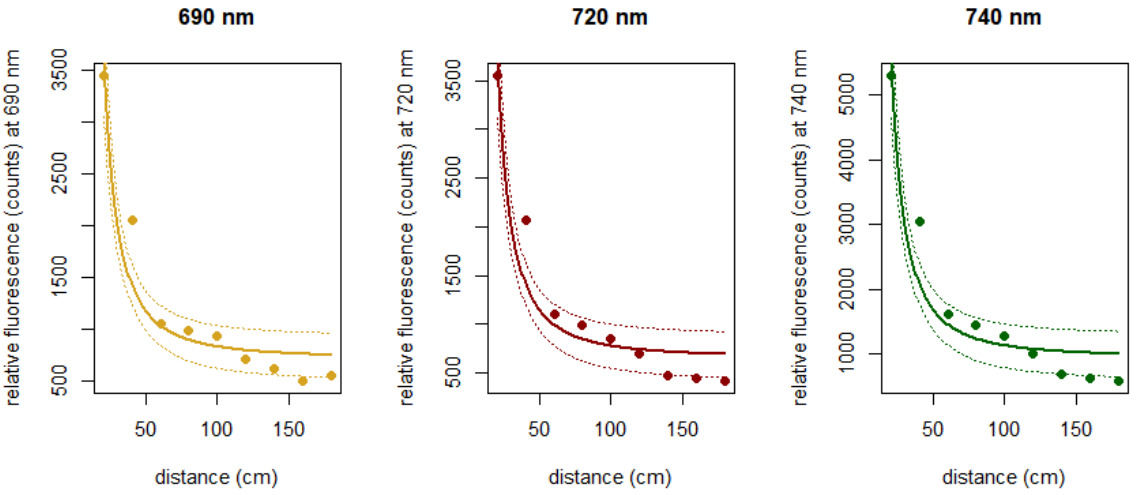

Figure 4.16: ChlF plotted against distance at 690 nm, 720 nm, and 740 nm. The line represents the inversed squared regression, the dotted lines show the 95% confidence interval. The ChlF is from the *pilea*, excited by 450 nm with a power of 29 mW.

Figure 4.17 shows the relationship between power and distance, when the power is changed and the measured ChlF signal is kept the same (mean = 0.74, sd = 0.04). Here, a decelerated increase is detected, where increase in power lead to a second order polynomial increase in distance to keep the same ChlF signal.

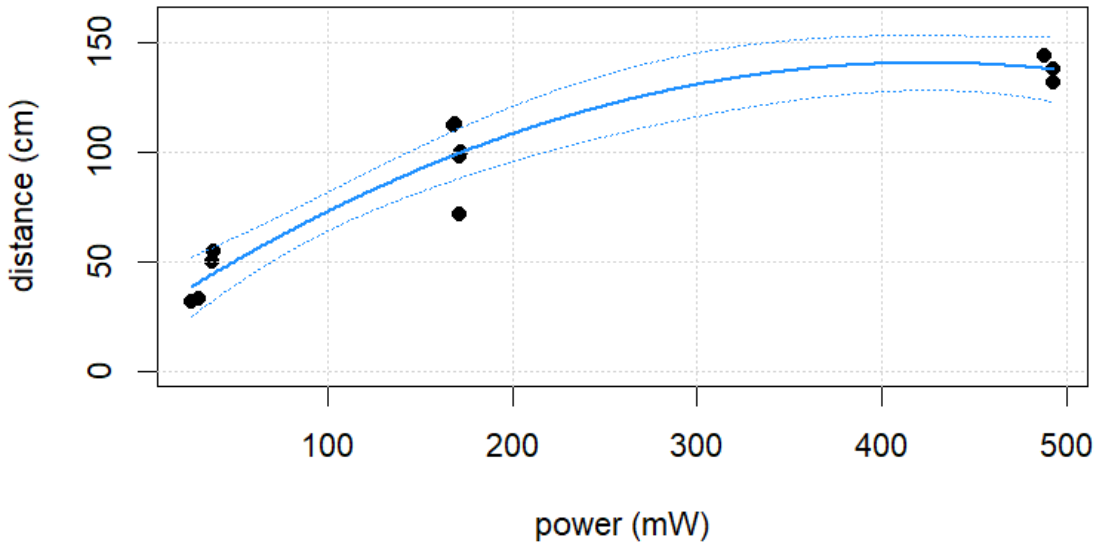

Figure 4.17: Relationship between laser power and distance when retrieving a similar FR_{max} ratio (mean = 0.74, sd = 0.04). The fitted line represents the fitted quadratic model, dotted lines present the 95% confidence interval.

In the figure, the line represents a fitted model of the second polynomial order. The fitted model has an adjusted R-squared of 0.90 with a p-value of 1.22e-5.

Power density

Power density is considered for remote applicability of the set-up as this is an important aspect of laser safety. Therefore, these results show how power density relates to ChlF parameters and the relative fluorescence intensity.

Figure 4.18 shows the relative fluorescence values for different power densities at wavelengths 690 nm, 720 nm, and 740 nm, collected with a laser power of 81 mW. The three plots all show a parabola-shaped relationship with the top around a power density of 100-150 mW/cm^2. The fitted functions yield an adjusted R-squared of 0.89 (p-value = 3.84e-11) for 690 nm, 0.84 (p-value = 1.53e-9) for 720 nm, and 0.81 (p-value = 1.33e-8) for 740 nm.

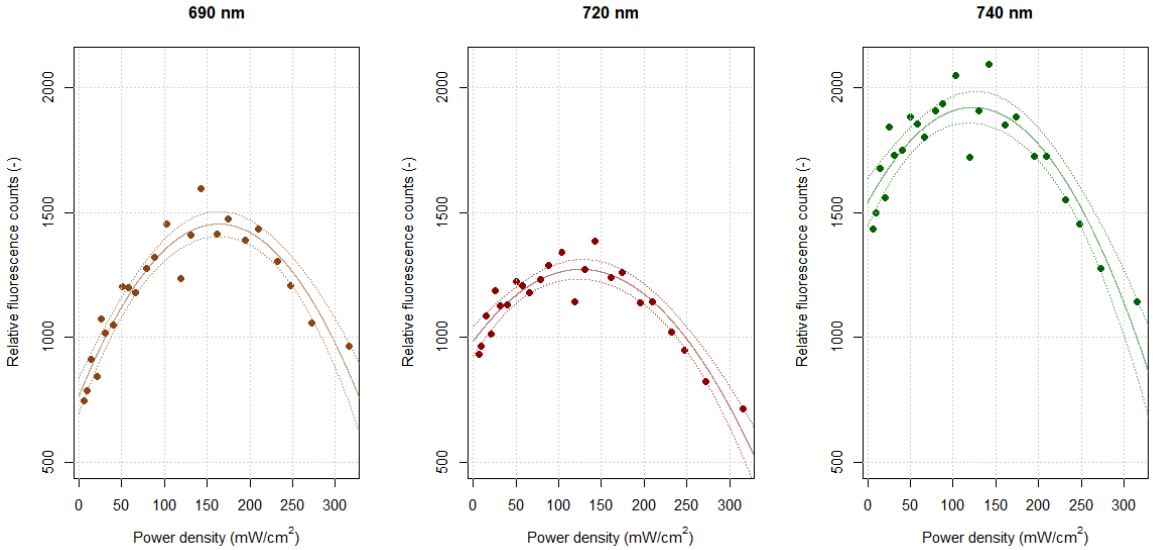

Figure 4.18: ChlF counts plotted against power density at 690 nm, 720 nm and 740 nm. Fitted line presents the second polynomial order relationship, dotted line presents the 95% confidence interval. ChlF data is collected with the 405 nm laser with 81 mW laser power at 80 cm distance, with various beam areas.

Figure 4.19 shows the yielded F_{690}/F_{730} ratio plotted against the power density, given in mW/cm^2. Measurements were taken from a distance of 80 cm. The figure shows a polynomial second-degree relationship between the power density and the ratio. The grey line represents the polynomial relationship fitted: the model has an adjusted R-squared of 0.99 with a significant p-value smaller than 2.2e-16.

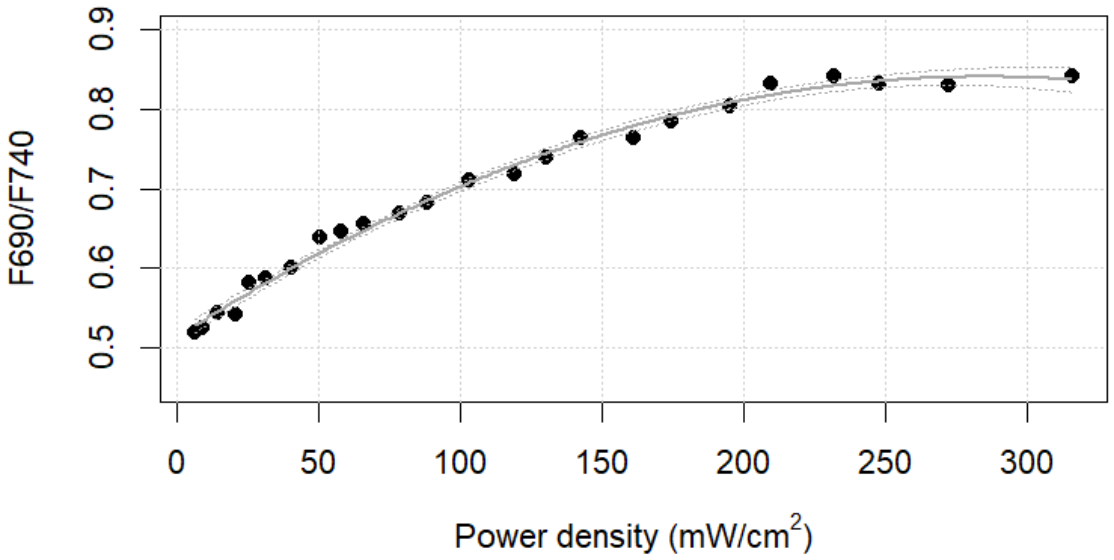

Figure 4.19: F_{690}/F_{740} values plotted against power density. Grey line presents the fitted second polynomial regression, the dotted lines present the 95% confidence interval.

5. Discussion

5.1. Significance of results

5.1.1: Literature review

Based on literature presented in section 2, optimal conditions for LIF research of vegetation are where the plants are cultivated and grown in a controlled environment, and water stress is controlled based on water potential of soils or leaves. These studies also often use destructive methods to measure leaf water potential or chlorophyll content. On the other hand, the literature review identified studies where the optimal conditions of plants were not considered as much but were more focussed on the technical abilities of the set-up they used. The literature review also showed that a variety of instruments are used to assess vegetation fluorescence. In the scope of this research, simple set-ups as presented in (Misra et al., 2021) show the possibility of using a low-cost set-up in real world scenario's and shows the potential for the set-up used in this study. Furthermore, this set-up has the possibility to be expanded further by adding RGB and hyperspectral cameras, or adding LiDAR (Du et al., 2020; Wang et al., 2018; Zhao et al., 2020).

5.1.2. Part 1: Leaf conditions and characteristics

Laser induced fluorescence of different plant species

The literature review shows the use of LIF can be used to derive various physiology parameters from vegetation. Next to the parameters used for plant physiology, differences between species can also be made, as shown by Yang et al. (2016). The spectra of the ChlF in Figure 4.1 show that the *iresine* and the *calathea* have a higher emission compared to the *coffea*, *pilea* and *viola* 1. The higher emission of the *iresine* and *calathea* can be explained by the lack of pigment (chlorophyll) – an increasing chlorophyll content in a leaf causes a decrease in ChlF emission (Buschmann, 2007; Leufen et al., 2014), which is shown by the lower fluorescence emission of the *coffea*, *pilea* and *viola.* However, the *viola* 1 shows, in comparison to the *pilea* and *coffea*, a high fluorescence ratio (Figure 4.3). The spectrum of the *viola* (Figure 4.1) show a much lower emission rate in the far-red peak compared to the *pilea* and *coffea*. This can be attributed to a lower chlorophyll content that the *viola* has compared to the *pilea* and *coffea*, as shown by the SPAD values in Figure 4.3. The increase in the far-red peak for an increasing chlorophyll content is stronger compared to a change in the red peak, hence the "shoulder" in the *viola* emission (Buschmann, 2007; Lichtenthaler et al., 1986). Furthermore, fluorescence emission is also dependent on the arrangement of cells in the leaf tissue (Borsuk & Brodersen, 2019; Buschmann, 2007). The leaf texture of the *coffea* and *pilea* is thicker than that of the *viola.* The thickness of the leaf might allow for deeper penetration of the light and thus more re-absorption, lowering the ChlF emission (Buschmann, 2007).

The spectra in Figure 4.2 show the same spectral behaviours but at different intensities. This could be due to the difference in chlorophyll content. However, this difference cannot be seen looking at the relative greenness recorded by the SPAD in Figure 4.3. Here, the higher recorder SPAD values of *viola* 5 and *viola* 6 suggest a higher relative greenness, whilst the high ChlF emission of these plants suggest a lower chlorophyll content. However, when looking at the relationship between the ChlF ratio and the SPAD (Figure 4.3), the correlation for all species, but also the one for the viola's specifically, shows a negative relationship. This suggest that a higher relative greenness relates to a lower ChlF ratio, which is in line with Lichtenthaler et al. (1986) and Buschmann et al. (2007), who state that a lower ratio value corresponds with a higher chlorophyll content due to the larger changes in fluorescence emissions in the far-red peak.

LIF of mature and young leaves + upper and lower side of leaves

Figure 4.4 compares the spectra of young and mature leaves of *coffea* (Figure 4.4A) and *viola* (Figure 4.4B). Both plants show a higher ChlF for the younger leaf than the mature leaf. This is in line with the fact that younger leaves have a lower chlorophyll content and thus a higher ChlF emission (Lichtenthaler et al., 1986). Furthermore, Figure 4.4C and Figure 4.4D compare the adaxial (upper side)

and abaxial (lower side) of the leaf. For both plants, the adaxial side shows a lower fluorescence emission. This can be attributed to the leaf structure and distribution of chlorophyll in the leaf. Here, the adaxial side has a higher chlorophyll content, so more reabsorption of light is detected and consequently lowers the ChlF emission in the red band. The abaxial sides of the leaf show an overall higher ChlF emission due to a lower chlorophyll content, and also a relatively higher emission in the red peak due to decrease of re-absorption (Buschmann, 2007). The findings derived from Figure 4.4 are also found by Chappelle et al. (1984), Gameiro et al. (2016), and Lichtenthaler et al. (1986).

Exploring LIF parameters

As mentioned earlier, the ratio between the red and far-red peak are used to assess chlorophyll content. Table 4.1 shows that while the absolute values for the ChlF ratios are different, they show the same information when making a relative comparison. This is between the ratios in the same state and between the states (F_s or F_m). The correlation matrix between the different ratios shows this as well – all have a very high correlation ($r > 0.965$)(Appendix B, Table B.0.1). This can be explained by the fact that similar data was used (the same spectra) only at different points in the peaks. The correlation between FR_{max} and F_{690}/F_{740} is 0.999, which is higher than the correlation between FR_{max} and F_{690}/F_{730} (0.965). Looking at the spectra in Figure 4.4, the values for the maximum peaks and the value at 740 nm lie closer together than the value of 730 nm and the maximum peak. The close proximity of 740 nm and F_m in the far-red can also explain the closeness of the data points as seen in Figure 4.5. Here, both F_{690}/F_{740} and FR_{max} show a higher correlation between steady state and saturating state than F_{690}/F_{730}. The results that show a higher comparability between the ratio's that lie closer to the maximum ChlF peaks is in line with earlier findings (Kharcheva, 2014). As the placement of the maximum ChlF peaks can be different for plant species, it can be argued that the use of FR_{max} gives the most representable results.

The other parameters related to photosynthesis do not display the same absolute values but show similarity in results (Table 4.2). This can also be seen in the correlation values between the photosynthesis parameters (Appendix B, Table B.0.2). The high correlation between Rfd and EQY can be attributed to the fact that the same variable (F_m and F_s) is used to calculate the values. The high correlation between Rfd and DFI might be due to the fact that Hsiao et al. (2010) used the Rfd parameter as validation for the DFI.

Comparing the different set of parameters (Appendix B, Table B.0.3), the correlation between the ratios and the photosynthesis parameters is very low but can be attributed to the different physiologies they measure. However, this shows that using the ratio is not interchangeable for the parameters related to the photosynthetic activity. Considering this finding in a real-world scenario, the photosynthesis parameters are not feasible due to the 4-minute duration of the measurement. While Hsiao et al. (2010) already tried to lower the measurement time by developing the DFI, it can be argued that the proposed 170 seconds is still an unfeasible measuring time in real-world applications using an aerial platform.

5.1.2. Part 2: Water stress

Fast stress

The results of the fast stress experiment show an increase in fluorescence counts between the beginning and end of the experiment (Figure 4.6), and a decrease in the ChlF ratio over time (Appendix D, Table D.0.1). The relationship between H% and the ChlF ratio is significant (Figure 4.7). These findings are in line with the findings of Gameiro et al. (2016), who reported an increase in fluorescence values with a decrease of the ChlF ratio for the fast stress experiment. This can be explained by the shrinkage of the leaf due to the water loss. As a consequence of the shrinkage, chloroplasts are grouped closer together. The higher concentration per area increases re-absorption in the red peak and a higher emission in the far-red, lowering the ChlF ratio (Buschmann, 2007; Gameiro et al., 2016). The SPAD values (Figure 4.8) show a slight increase in relative greenness between the start and end of the experiment, however no significant difference was found. The slight difference could also be attributed to the leaf shrinkage. However, it shows that ChlF is more sensitive to changes compared to the SPAD, suggesting the possibility for early detection of stress.

Slow stress

The induced drought for the slow stress experiment is shown in **Error! Reference source not found.** and is intuitive because the experiment group endured significant water loss. However, this is based on the total weight of the plant, soil, and pot. Even though the experiment ran longer compared to that of Gameiro et al. (2016) (14 days of drought induction compared to 12 days in Gameiro et al. (2016)), the stressed plants reached a water content of 43% (viola 3) and 39% (viola 4), while the stressed plant from Gameiro et al. (2016) reached a soil water content of approximately 20%. Assuming the approach taken in this research is comparable to the soil water content, the plants used in this research were less stressed compared to Gameiro et al. (2016). Looking at the leaf level, the fluorescence emission of viola 4 is reduced at the end of the experiment compared to the start (Figure 4.9). This is in line with the findings from Gameiro et al. (2016), who concluded that the decrease in fluorescence emission can be attributed to the water stress of the plant. However, little difference is found between the fluorescence spectra for viola 3, which is not in line with the expectation. Additionally, viola 2 also shows a decrease in fluorescence spectra, so while this plant belonged to the control group, the spectra suggest an increase in stress.

When the F_{690}/F_{730} ratio of the stressed group is plotted against the water content, the relationship between H% and the ratio are opposing. Viola 3 shows a moderate relationship where the ratio shows a slight increase with decreasing H%, although the linear regression shows that this is not a significant increase. In contrast, viola 4 shows a significant decrease in ratio with a decreasing water content. However, while the overall reduction in ChlF emission (Figure 4.9) is in line with the findings of Gameiro et al. (2016), their results show an increase of the ratio with an increased stress. This suggest that changes in the fluorescence peaks due to stress are different between the viola and Arabidopsis (the plant species used by Gameiro et al. (2016). The red peak in this study shows a more pronounced change in the violas compared to the far-red peak, while this behaviour is reversed for Gameiro et al. (2016). Fedotov et al. (2017) also found that the ratio of plants in a stressed state is higher compared to normal plants. However, on the other hand, Lichtenthaler et al. (1986) shows a decrease in the ratio between the red and far-red peak for stressed soybean plant. An explanation for the decrease in the ratio might be that due to the stress of the plant, more energy is transferred to PSI and thus the far-red peak of the ChlF, related to PSI, increases, lowering the ChlF ratio values (Buschmann, 2007). However, the literature does report contrasting results, suggesting that ChlF changes differently for different plant species when subjected to water stress.

Looking on a canopy level, the spectra shown in Figure 4.12 show similar spectra for the control group over time and a lower spectrum at the end of the experiment for the stressed group. This is in line with the finding on a leaf level (Figure 4.9).

Figure D.0.3 (Appendix D) shows the F_{690}/F_{730} ratio values of the canopy measurements between the start and the end of the experiment. While not significant, the control group (viola 1 and 2) show an increase in ChlF. This could be due to new growth where younger leaves have a lower chlorophyll content than older leaves, as discussed before (Buschmann, 2007). Because of the measurement capturing the canopy instead of one leaf, new growth at the top of the canopy is measured as well. Both stressed plants show a decrease in ChlF ratio between the first and last day, where only viola 4 shows a significant decrease. This could be due to shrinkage of the leaves under water stress and therefore increasing the chlorophyll content per area and thus causing a lower ChlF ratio, as seen by the fast stress experiment (Buschmann, 2007; Gameiro et al., 2016). However, another explanation could be the increase of energy to PSI, increasing the peak in the far-red and thus lowering the ChlF ratio, as suggested by the leaf level stress (Buschmann, 2007).

Literature shows that scaling fluorescence measurements to a canopy level introduces more factors to consider that might affect the fluorescence signal. Atherton et al. (2016) states that the fluorescence signal is sensitive to the leaf inclination angle. Additionally, the red ChlF signal is more dependent on the top layer of the canopy level, whilst the far-red ChlF signal might have a bigger contribution from deeper layers of the canopy (Cendrero-Mateo et al., 2016). Re-absorption and multi-scattering will affect the measured ChlF signal on a canopy level. Furthermore, when measuring stress using ChlF, Wu et al. (2016) found that the ChlF decline due to drought occurred more rapidly in lower hanging leaves of the plant compared to the upper leaves. This could also affect stress detection of plants for canopy measurements. Lastly, scaling up to canopy level can also make soil fluorescence part of the measurements. While the signal is low, it is still important to consider when scaling to canopy

measurements (Fedotov et al., 2017). The various factors mentioned here can be the explanation as to why the correlation between the ChlF ratio of the leaf level and canopy level is very low (Appendix D, Figure D.0.4). However, looking at only viola 4, a strong relationship between leaf and canopy measurements is found. For this result, especially due to the low correlation in the other plants, no explanation is found in literature.

5.1.2. Part 3: Remote applicability

The high fit of the inversed squared regression in Figure 4.16 confirms the expected relationship between fluorescence intensity and distance, referred to as the inverse squared law (Marti-Lopez et al., 2004). Figure 4.17 shows that to retrieve good signal at further distance, more laser power is needed to obtain the same signal intensity.

Considering the power density when measuring fluorescence, a parabolic relationship exists between power density and fluorescence intensity (Figure 4.18). The reason for this could be because with a high-power density a small area is excited, so less fluorescence is emitted. Lowering the power density (so increasing the area) excited a larger leaf area, leading to more fluorescence emission, until a point is passed where the power density gets too low to retrieve a good signal. Figure 4.18 shows that it can be argued that there is an optimum for power density where there is a trade-off between lowering the power density while still yielding a good signal. Moreover, a large leaf (diameter of approximately 7.2cm) of the *pilea* was excited for the experiment presented in Figure 4.18. However, increasing the area on smaller leaves may not show the same results, as the increased excitation area may excite not only the target leaf, but also soil background or other leaves, which might have an effect on the acquired signal.

Figure 4.19 shows that with increasing power density the ratios get to a saturating point. This can be brought back to Figure 4.18. Here, the 690 nm parabola is more symmetrical compared to the 740 nm plot. The latter yields higher fluorescence values at a low power density than at a high-power density. One explanation could be that the higher power density makes the light penetrate deeper to the leaf, so more re-absorption takes place, leading to a relatively higher emission in the far-red peak.

.

5.2. Limitations and uncertainties

This research shows various aspects of measuring LIF and relationship between different variables related to photosynthesis, chlorophyll content, water stress, measuring distance and power density. However, it is important to mention the limitations of the scope of this research and shed light on aspects that were not considered here, while being of importance to measuring ChlF.

First, the limitations related to data collection. As mentioned in the methods, the correction of the acquired laser spectra is suboptimal and might have influenced the overall outcome. Still, even though this study is based on relative comparisons rather than absolute, it is important to note that the data processing of this study is not done according to standard protocol, as done by for example (Lednev et al., 2022a). Next to that, the study was done on a small group of plants. For example, statement made related to the different ChlF spectra of different species are based on individual plants, rather than a comparison of groups of different species. Therefore, measurement errors might have a bigger impact compared to studies of larger groups. Additionally, it is important to mention that the statistical tests used in this research assume normality. The normality is often obtained when using large datasets – however, due to the small sample sizes of the data used, it is possible that not all assumptions of the statistical tests are met. Nonetheless, results are still supported by literature findings.

Second, the plants used in this study were subjected to various conditions, in contrast to the standard conditions found and mentioned in the literature review. Due to changes in environment, the plants did not have a consistent watering schedule. Therefore, the “ground truth” weight of the plant as indicator for water content is assumed to be the ground truth, but it is possible that plant may have been overwatered, or not in optimal healthy conditions.

Third, this research lacks a validation method of the acquired fluorescence data. Results are only validated by making a comparison with earlier findings from literature and using SPAD measurements. However, SPAD only measures relative greenness, thus comparison between species or

to other parameters should be done with care (Uddling et al., 2007). Thus, an accuracy assessment is lacking. Still, the results are comparable with findings in literature. This at least means that the experimental approach that is taken in this study is worth exploring further. A validation method and accuracy assessment for any follow-up research is highly recommended.

Finally, the experimental approach of the study did not consider variables that are mentioned in literature that affect the ChlF. For example, leaf angle inclination was attempted to keep as perpendicular to the laser beam as possible, but not strictly considered since leaf angles were not easily manipulated for in vivo measurements. However, the incident light angle is shown to influence ChlF measurements (Cendrero-Mateo et al., 2016). Next to that, an important attention point in LIF applications to real-world scenario's is the effect of background light from the sun on the fluorescence measurements. While the effect from distance and power density was considered in indoor conditions, real world environmental conditions, such as sunlight, but also temperature that might affect ChlF (Buschmann, 2007), were not considered in the scope of this research.

6. Conclusion

This research explores various aspects to applying laser induced ChlF measurement in real-world scenarios for monitoring vegetation health. The experiments were performed in controlled lab environment and over-the-counter plants were used as target objects. Non-imaging spectrometer was used to measure the fluorescence response and various statistical analysis methods were in the post processing step to deduce meaningful interpretation of the measurements.

The results show that the FR_{max} ratio might be the best applicable ratio when measuring for various plant species, as this accounts for differences of the place of red and far-red peaks in the spectra. Furthermore, the ChlF ratios showed a high correlation between ratios based on steady state and saturating spectra, suggesting that 4-minute measurements in the field are not needed to retrieve valuable ChlF ratios. However, results did show that the ChlF ratios and the photosynthetic parameters EQY, Rfd and DFI are not comparable. Considering a real-world application, further research is needed to find a way to quantify these photosynthetic related parameters.

Furthermore, the research explored the identification of water stress in plants using the designed controlled set-up. For the dissected leaves in the fast stress experiment, significant values were found. However, the slow stress experiment shows the potential of the set-up for early detection of stress, but the robustness of the results needs further research due to the small dataset and the lack of a truly controlled environment regarding plant care and stress induction.

Lastly, real-world applicability of LIF of vegetation was investigated where the variables of distance and power density were explored. The results of the distance experiments presented the loss of signal related to the inverse squared law, and the need for an increase in laser power when increasing distance to be able to still yield detectable ChlF measurements. The power density experiments showed the probability of an optimum when retrieving ChlF values, were there is a possible trade-off between area increase for more excitation, and area decrease for a better signal. In line with that, when calculating the ChlF ratio for different densities, a saturation was identified as the power density is increasing.

In conclusion, the experimental approach as evaluated in this research shows that the proposed design of the LIF set-up can be used to retrieve valuable information related to plant physiology. However, more research related to real-world application to assess the real-world applicability, combined with a deeper understanding of LIF of vegetation using validation methods is needed. Nonetheless, this research has shown the potential of LIF vegetation measurements in a real-world scenario.

7. Recommendations

In this research some limitations are identified in the experimental design that are recommended to be improved in any follow-up research.

Firstly, as mentioned before, the results of the research are tested by means of comparison, but validation is lacking. While the results are comparable to results found in literature, it is highly recommended to incorporate a validation method to assess the accuracy of the proposed LIF set-up. Furthermore, the larger sample size of vegetation and a steadier and more controlled environment for these plants is recommended to ensure more robustness of results in follow-up research.

Next to that, literature mentions variables such as sunlight, temperature, and leaf angle that influence the acquisition of the ChlF signal (Buschmann, 2007; Cendrero-Mateo et al., 2016). However, these variables are not considered in this research. Since these variables are shown to influence ChlF measurements, and are present in real-world environments, future research is strongly suggested to explore the effect on these variables to explore the applicability of LIF remote sensing further.

Finally, from this research rise more questions that are worth exploring further. Firstly, various laser hazard variables are discussed in the literature review (MPE, intrabeam NOHD, diffuse NHZ). The set-up allows for beam area manipulation, making it possible to confirm to a safe MPE. However, ChlF signals were retrieved without considering a safe MPE. The two other laser hazard variables were not considered at all. Here, the question arises whether the LIF set-up is applicable in real-world scenarios from a laser-safety perspective.

Furthermore, the discussion mentions that while the set-up can be used to derive photosynthesis related variables, such as Rfd and EQY, a measuring time of four minutes to retrieve the F_s is not feasible in real-world applications. While the DFI lowers the measuring time, it can still be considered too long for a real-world application. It is recommended for future research to explore other ways to quantify photosynthetic activity with a shorter measuring time.

Lastly, the different behaviour of species under drought stress are recommended to consider for real-world scenarios. While this study showed a decrease in ChlF ratio under stress, Gameiro et al. (2016) showed an increase in ChlF ratio under water stress. If LIF is used on various species which react differently under stress regarding fluorescence emission, a type of generalisation, independent of species, or a way to differentiate between species fluorescent behaviour needs to be explored to ensure an accurate monitoring approach of vegetation health.

References

Arief, M. A. A., Kim, H., Kurniawan, H., Nugroho, A. P., Kim, T., & Cho, B.-K. (2023). Chlorophyll Fluorescence Imaging for Early Detection of Drought and Heat Stress in Strawberry Plants. *Plants*, *12*(6), 1387. https://doi.org/10.3390/plants12061387

Atherton, J., Nichol, C. J., & Porcar-Castell, A. (2016). Using spectral chlorophyll fluorescence and the photochemical reflectance index to predict physiological dynamics. *Remote Sensing of Environment*, *176*, 17–30. Scopus. https://doi.org/10.1016/j.rse.2015.12.036

Barat, K. (2019). *Laser Safety: Practical Knowledge and Solutions*. IOP Publishing.

Barták, M., Trnková, K., Hansen, E. S., Hazdrová, J., Skácelová, K., Hájek, J., & Forbelská, M. (2015). Effect of dehydration on spectral reflectance and photosynthetic efficiency in Umbilicaria arctica and U. hyperborea. *Biologia Plantarum*, *59*(2), 357–365. https://doi.org/10.1007/s10535-015-0506-1

Beleites, C., & Sergo, V. (n.d.). *hyperSpec: A packaga to handle hyperspectral data sets in R.* (0.100.0) [R package version 0.100.0]. https://github.com/r-hyperspec/hyperSpec

Bian, X. (2022). Spectral Preprocessing Methods. In X. Chu, Y. Huang, Y.-H. Yun, & X. Bian, *Chemometric Methods in Analytical Spectroscopy Technology* (pp. 111–168). Springer Nature Singapore. https://doi.org/10.1007/978-981-19-1625-0_4

Borsuk, A. M., & Brodersen, C. R. (2019). The Spatial Distribution of Chlorophyll in Leaves. *Plant Physiology*, *180*(3), 1406–1417. https://doi.org/10.1104/pp.19.00094

Boussadia, O., Steppe, K., Van Labeke, M.-C., Lemeur, R., & Braham, M. (2015). Effects of Nitrogen Deficiency on Leaf Chlorophyll Fluorescence Parameters in Two Olive Tree Cultivars 'Meski' and 'Koroneiki.' *Journal of Plant Nutrition*, *38*(14), 2230–2246. https://doi.org/10.1080/01904167.2015.1069339

Buschmann, C. (2007). Variability and application of the chlorophyll fluorescence emission ratio red/far-red of leaves. *Photosynthesis Research*, *92*(2), 261–271. https://doi.org/10.1007/s11120-007-9187-8

Cendrero-Mateo, M. P., Moran, M. S., Papuga, S. A., Thorp, K. R., Alonso, L., Moreno, J., Ponce-Campos, G., Rascher, U., & Wang, G. (2016). Plant chlorophyll fluorescence: Active and passive measurements at canopy and leaf scales with different nitrogen treatments. *Journal of Experimental Botany*, *67*(1), 275–286. https://doi.org/10.1093/jxb/erv456

Chappelle, E. W., Wood, F. M., McMurtrey, J. E., & Newcomb, W. W. (1984). Laser-induced fluorescence of green plants 1: A technique for the remote detection of plant stress and species differentiation. *Applied Optics*, *23*(1), 134. https://doi.org/10.1364/AO.23.000134

Cogliati, S., Verhoef, W., Kraft, S., Sabater, N., Alonso, L., Vicent, J., Moreno, J., Drusch, M., & Colombo, R. (2015). Retrieval of sun-induced fluorescence using advanced spectral fitting

methods. *Remote Sensing of Environment*, *169*, 344–357. https://doi.org/10.1016/j.rse.2015.08.022

Cord, A. F., Brauman, K. A., Chaplin-Kramer, R., Huth, A., Ziv, G., & Seppelt, R. (2017). Priorities to Advance Monitoring of Ecosystem Services Using Earth Observation. *Trends in Ecology & Evolution*, *32*(6), 416–428. https://doi.org/10.1016/j.tree.2017.03.003

Donaldson, L. (2020). Autofluorescence in Plants. *Molecules*, *25*(10), 2393. https://doi.org/10.3390/molecules25102393

Du, L., Shi, S., Yang, J., Wang, W., Sun, J., Cheng, B., Zhang, Z., & Gong, W. (2017). Potential of spectral ratio indices derived from hyperspectral LiDAR and laser-induced chlorophyll fluorescence spectra on estimating rice leaf nitrogen contents. *Optics Express*, *25*(6), 6539. https://doi.org/10.1364/OE.25.006539

Du, L., Yang, J., Chen, B., Sun, J., Chen, B., Shi, S., Song, S., & Gong, W. (2020). Novel Combined Spectral Indices Derived from Hyperspectral and Laser-Induced Fluorescence LiDAR Spectra for Leaf Nitrogen Contents Estimation of Rice. *Remote Sensing*, *12*(1), 185. https://doi.org/10.3390/rs12010185

Fang, X.-X., Li, H.-Y., Fang, P., Pan, J.-Z., & Fang, Q. (2016). A handheld laser-induced fluorescence detector for multiple applications. *Talanta*, *150*, 135–141. https://doi.org/10.1016/j.talanta.2015.12.018

Fedotov, Y., Belov, M. L., Bullo, O. A., & Gorodnichev, V. (2017). Experimental research of different factors influencing on stability of laser induced fluorescence spectra of plants. In O. A. Romanovskii & G. G. Matvienko (Eds.), *23rd International Symposium on Atmospheric and Ocean Optics: Atmospheric Physics* (p. 62). SPIE. https://doi.org/10.1117/12.2285291

Fernandez-Jaramillo, A. A., Duarte-Galvan, C., Contreras-Medina, L. M., Torres-Pacheco, I., Romero-Troncoso, R. D. J., Guevara-Gonzalez, R. G., & Millan-Almaraz, J. R. (2012). Instrumentation in Developing Chlorophyll Fluorescence Biosensing: A Review. *Sensors*, *12*(9), 11853–11869. https://doi.org/10.3390/s120911853

Gameiro, C., Utkin, A. B., Cartaxana, P., Silva, J. M. D., & Matos, A. R. (2016). The use of laser induced chlorophyll fluorescence (LIF) as a fast and non-destructive method to investigate water deficit in Arabidopsis. *Agricultural Water Management*, *164*, 127–136. https://doi.org/10.1016/j.agwat.2015.09.008

Guidi, L., Lo Piccolo, E., & Landi, M. (2019). Chlorophyll Fluorescence, Photoinhibition and Abiotic Stress: Does it Make Any Difference the Fact to Be a C3 or C4 Species? *Frontiers in Plant Science*, *10*, 174. https://doi.org/10.3389/fpls.2019.00174

Hsiao, S.-C., Chen, S., Yang, I.-C., Chen, C.-T., Tsai, C.-Y., Chuang, Y.-K., Wang, F.-J., Chen, Y.-L., Lin, T.-S., & Lo, Y. M. (2010). Evaluation of plant seedling water stress using dynamic fluorescence index with blue LED-based fluorescence imaging. *Computers and Electronics in Agriculture*, *72*(2), 127–133. https://doi.org/10.1016/j.compag.2010.03.005

Kautz, B., Noga, G., & Hunsche, M. (2014). Sensing drought- and salinity-imposed stresses on tomato leaves by means of fluorescence techniques. *Plant Growth Regulation*, *73*(3), 279–288. https://doi.org/10.1007/s10725-014-9888-x

Kharcheva, A. V. (2014). *Fluorescence intensities ratio F685/F740 for maple leaves during seasonal color changes and with fungal infection* (E. A. Genina, V. L. Derbov, I. Meglinski, & V. V. Tuchin, Eds.; p. 90310S). https://doi.org/10.1117/12.2049509

Kolber, Z., Klimov, D., Ananyev, G., Rascher, U., Berry, J., & Osmond, B. (2005). Measuring photosynthetic parameters at a distance: Laser induced fluorescence transient (LIFT) method for remote measurements of photosynthesis in terrestrial vegetation. *Photosynthesis Research*, *84*(1–3), 121–129. https://doi.org/10.1007/s11120-005-5092-1

Kölbl, C., Diedrich, M., Ellingen, E., Duschek, F., Selim, M., & Berkelmann-Löhnertz, B. (2023). Remote detection of fungal pathogens in viticulture using laser-induced fluorescence: An experimental study on infected potted vines. *Frontiers in Horticulture*, *2*, 1185468. https://doi.org/10.3389/fhort.2023.1185468

Lednev, V. N., Grishin, M. Ya., Sdvizhenskii, P. A., Kurbanov, R. K., Litvinov, M. A., Gudkov, S. V., & Pershin, S. M. (2022b). Fluorescence Mapping of Agricultural Fields Utilizing Drone-Based LIDAR. *Photonics*, *9*(12), 963. https://doi.org/10.3390/photonics9120963

Lednev, V. N., Grishin, M. Ya., Sdvizhenskii, P. A., Pershin, S. M., Zavozin, V. A., Kurbanov, R. K., & Litvinov, M. A. (2022a). Ultracompact fluorescence LIDAR for drone based autonomous monitoring in agriculture. *2022 International Conference Laser Optics (ICLO)*, 1–1. https://doi.org/10.1109/ICLO54117.2022.9840297

Leufen, G., Noga, G., & Hunsche, M. (2014). Fluorescence Indices for the Proximal Sensing of Powdery Mildew, Nitrogen Supply and Water Deficit in Sugar Beet Leaves. *Agriculture*, *4*(2), 58–78. https://doi.org/10.3390/agriculture4020058

Li, C., Peng, L., Zhou, M., Wei, Y., Liu, L., Li, L., Liu, Y., Dou, T., Chen, J., & Wu, X. (2022). SIF-Based GPP Is a Useful Index for Assessing Impacts of Drought on Vegetation: An Example of a Mega-Drought in Yunnan Province, China. *Remote Sensing*, *14*(6), 1509. https://doi.org/10.3390/rs14061509

Lichtenthaler, H. K., Buschmann, C., & Knapp, M. (2005). How to correctly determine the different chlorophyll fluorescence parameters and the chlorophyll fluorescence decrease ratio R_{Fd} of leaves with the PAM fluorometer. *Photosynthetica*, *43*(3), 379–393. https://doi.org/10.1007/s11099-005-0062-6

Lichtenthaler, H. K., Buschmann, C., Rinderle, U., & Schmuck, G. (1986). Application of chlorophyll fluorescence in ecophysiology. *Radiation and Environmental Biophysics*, *25*(4), 297–308. https://doi.org/10.1007/BF01214643

Marti-Lopez, L., Bouza-Dominguez, J., Hebden, J. C., & Martinez-Celorio, R. A. (2004). *Deriving the inverse square law from radiative transfer equations* (A. Marcano O. & J. L. Paz, Eds.; pp. 45–50). https://doi.org/10.1117/12.589362

Misra, A. K., Acosta-Maeda, T. E., Zhou, J., Egan, M. J., Dasilveira, L., Porter, J. N., Rowley, S. J., Zachary Trimble, A., Boll, P., Sandford, M. W., McKay, C. P., & Nurul Abedin, M. (2021). Compact Color Biofinder (CoCoBi): Fast, Standoff, Sensitive Detection of Biomolecules and Polyaromatic Hydrocarbons for the Detection of Life. *Applied Spectroscopy*, *75*(11), 1427–1436. https://doi.org/10.1177/00037028211033911

Pérez-Bueno, M. L., Pineda, M., & Barón, M. (2019). Phenotyping Plant Responses to Biotic Stress by Chlorophyll Fluorescence Imaging. *Frontiers in Plant Science*, *10*. Scopus. https://doi.org/10.3389/fpls.2019.01135

Pérez-Bueno, M., Pineda, M., Cabeza, F., & Barón, M. (2016). Multicolor Fluorescence Imaging as a Candidate for Disease Detection in Plant Phenotyping. *FRONTIERS IN PLANT SCIENCE*, *7*. https://doi.org/10.3389/fpls.2016.01790

Shamsi, E., Parvin, P., Ahmadinouri, F., & Khazai, S. (2023). Laser-induced fluorescence spectroscopy of plant-based drugs: Opium and hashish provoking at 405 nm. *Spectrochimica Acta Part A: Molecular and Biomolecular Spectroscopy*, *302*, 123055. https://doi.org/10.1016/j.saa.2023.123055

Smorenburg, K., Courreges-Lacoste, G. B., Berger, M., Buschman, C., Court, A. J., Del Bello, U., Langsdorf, G., Lichtenthaler, H. K., Sioris, C., Stoll, M.-P., & Visser, H. (2002). *Remote sensing of solar-induced fluorescence of vegetation* (M. Owe & G. D'Urso, Eds.; p. 178). https://doi.org/10.1117/12.454193

Taylor, A. T., & Lai, E. P. C. (2021). Current State of Laser-Induced Fluorescence Spectroscopy for Designing Biochemical Sensors. *Chemosensors*, *9*(10), 275. https://doi.org/10.3390/chemosensors9100275

Truax, K., Dulai, H., Misra, A., Kuhne, W., Fuleky, P., Smith, C., & Garces, M. (2023). Laser-Induced Fluorescence for Monitoring Environmental Contamination and Stress in the Moss Thuidium plicatile. *Plants*, *12*(17), 3124. https://doi.org/10.3390/plants12173124

Uddling, J., Gelang-Alfredsson, J., Piikki, K., & Pleijel, H. (2007). Evaluating the relationship between leaf chlorophyll concentration and SPAD-502 chlorophyll meter readings. *Photosynthesis Research*, *91*(1), 37–46. https://doi.org/10.1007/s11120-006-9077-5

Wang, X., Duan, Z., Brydegaard, M., Svanberg, S., & Zhao, G. (2018). Drone-based area scanning of vegetation fluorescence height profiles using a miniaturized hyperspectral lidar system. *Applied Physics B*, *124*(11), 207. https://doi.org/10.1007/s00340-018-7078-7

Wu, C. W., Lee, M. C., Peng, Y. L., Chou, T. Y., Lin, K. H., & Chang, Y. S. (2016). Chlorophyll fluorescence upper-to-lower-leaf ratio for determination of irrigation time for Pentas lanceolata. *Photosynthetica*, *54*(2), 193–200. https://doi.org/10.1007/s11099-015-0175-5

Yang, J., Gong, W., Shi, S., Du, L., Zhu, B., Sun, J., & Song, S. (2016). Excitation Wavelength Analysis of Laser-Induced Fluorescence LiDAR for Identifying Plant Species. *IEEE Geoscience and Remote Sensing Letters*, *13*(7), 977–981. https://doi.org/10.1109/LGRS.2016.2557484

Yang, J., Song, S., Du, L., Shi, S., Gong, W., Sun, J., & Chen, B. (2018). Analyzing the Effect of Fluorescence Characteristics on Leaf Nitrogen Concentration Estimation. *Remote Sensing*, *10*(9), 1402. https://doi.org/10.3390/rs10091402

Zhang, J., Huang, Y., Pu, R., Gonzalez-Moreno, P., Yuan, L., Wu, K., & Huang, W. (2019). Monitoring plant diseases and pests through remote sensing technology: A review. *Computers and Electronics in Agriculture*, *165*, 104943. https://doi.org/10.1016/j.compag.2019.104943

Zhao, X., Shi, S., Yang, J., Gong, W., Sun, J., Chen, B., Guo, K., & Chen, B. (2020). Active 3D Imaging of Vegetation Based on Multi-Wavelength Fluorescence LiDAR. *Sensors*, *20*(3), 935. https://doi.org/10.3390/s20030935

Appendix A: Experiment overview

Table A.0.1: Overview of the experiments conducted in this research. Column experiment gives the name of the experiment; "date" gives the date(s) that the data was acquired; "plant" gives which plant(s) were used during the experiments; "laser settings" give the laser settings, consisting of laser excitation wavelength (Wl), laser power (P), integration time (int. time), averaging and boxcar; "settings" gives the specifications of environment (indoor is with lights turned on, dark is with the lights turned off), measuring distance (distance), and beam spot diameter (diameter); "Notes" gives any other notes about the experiments.

Experiment	**Date**	**Plant**	**Laser settings**	**Settings**	**Notes**
A: LIF of different species	2024-02-20	*Coffea*, *calathea*, *iresine*, *pilea*, *violas* 1-6	Wl: 405 nm, P: 159 mW, Int. time: 500 ms, Averaging 1, boxcar 0	Indoor environment; Distance 72 cm, Diameter 12 mm	In vivo
B: Mature/young leaves + adaxial & abaxial	2024-02-21	*Coffea*, *viola* 6	Wl: 405 nm, P: 164 mW, Int. time: 500 ms, Averaging 1, boxcar 0	Indoor environment; Distance 80 cm; Diameter 12 mm	In vitro
C: Fast stress	2024-03-05	*Viola* 5	Wl: 405 nm; P: 81 mW, Int. time: 500 ms, Averaging 1, boxcar 0	Indoor environment; Distance 80 cm; Diameter 12 mm	In vitro, detached leaves were measured every hour. Dried at room temperature (20 ˚C)
D: Slow stress	2024-03-05 2024-03-06 2024-03-07 2024-03-08 2024-03-11 2024-03-12 2024-03-13 2024-03-14	*Violas* 1-4	Wl: 405 nm; P (in mW, same order as dates): 82, 81, 77, 82, 80, 78, 81, 79; Int. time: 500 ms, Averaging 1, boxcar 0	Indoor environment; 80 cm distance; Diameter 15 mm (leaf level), 40 mm (canopy level)	In vivo, *violas* 1 and 2 belonged to the control group, *violas* 3 and 4 were subjected to water stress. Leaf as well as canopy measurements were taken.
E: Distance	2023-12-11	*Pilea*	Wl: 450 nm; P: 29 mW Int. time: 500 ms Averaging 1, boxcar 0	Indoor environment; Distances (in cm): 20, 40, 60, 80, 100, 120, 140, 160, 180;	In vivo, no diameter was recorder as the 450 nm laser is a point laser, and power density is assumed to be negligible.
E: Distance	2024-02-26	*Pilea*	Wl: 450 nm;	Indoor and dark environment.	

			P (in mW): 26, 30, 37, 38, 168, 169, 171, 172, 488, 493; Int. time: 500 ms; Averaging 1, boxcar 0.	Distances (in cm): 32, 33, 50, 55, 72, 98, 100, 112, 113, 132, 138, 144.	
F: Power density	2024-03-12	*Pilea*	Wl: 405 nm; P: 47 mW, 81 mW; Int. time: 500 ms Averaging 1, boxcar 0	Indoor environment; 80 cm distance; Diameters (in mm): 9, 10, 12, 15, 16, 18, 19, 20, 21, 22, 23, 24, 25, 27, 28, 30, 32, 35, 37, 40, 43, 45, 47, 50, 52, 55, 57, 60, 62, 65, 70	In vivo

Table A.0.2: Table of content of research data zip-file. First file (README.txt) is a description of the content of the zip-file. The pdf file is the final report. The other lines are folders; their contents will be explained in the README.

README.txt
VerhoekAE_ThesisReportGIRS2024-51_20240515.pdf
Presentations
Data
Figures_Tables
Scripts
Literature

Appendix B: Correlation matrices

Table B.0.1: Correlation matrix for parameters presented in Table 3.1. Red denotes the lowest correlation value, and green the highest correlation value.

	FR_{max}	F_{690}/F_{730}	F_{690}/F_{740}
FR_{max}	1	0.965	0.999
F_{690}/F_{730}		1	0.973
F_{690}/F_{740}			1

Table B.0.2: Correlation matrix of the EQY, Rfd, and DFI values as presented in Table 4.2. Conditional formatting is applied where a gradient from red-yellow-green highlights low to high correlation values between DFI, EQY and Rfd. Note that correlations within a parameter are not considered in the conditional formatting. The table shows the highest correlation between the EQY and Rfd parameters, and the lowest correlations between DFI and EQY.

	DFI_{690}	**DFI_{720}**	**DFI_{740}**	**EQY_{690}**	**EQY_{720}**	**EQY_{740}**	**Rfd_{690}**	**Rfd_{720}**	**Rfd_{740}**
DFI_{690}	1	0.991	0.992	0.778	0.766	0.761	0.868	0.809	0.807
DFI_{720}		1	0.983	0.752	0.758	0.745	0.851	0.807	0.795
DFI_{740}			1	0.797	0.788	0.786	0.877	0.821	0.824
EQY_{690}				1	0.985	0.985	0.973	0.978	0.987
EQY_{720}					1	0.996	0.948	0.989	0.993
EQY_{740}						1	0.938	0.975	0.988
Rfd_{690}							1	0.971	0.968
Rfd_{720}								1	0.993
Rfd_{740}									1

Table B.0.3: Correlation values between ChlF ratios and photosynthesis parameters. Conditional formatting is applied where a gradient from red-yellow-green highlights low to high correlation values found in the table. The table shows that ratios calculated with Fs values have a lower correlation with the photosynthesis parameters than the ratios calculated with F_m. For both states, DFI shows a lower correlation with the ChlF ratios than EQY and Rfd.

	F_s			**F_m**		
	FR_{max}	**F_{690}/F_{730}**	**F_{690}/F_{740}**	**FR_{max}**	**F_{690}/F_{730}**	**F_{690}/F_{740}**
DFI_{690}	-0.077	-0.261	-0.127	0.131	0.033	0.093
DFI_{720}	-0.047	-0.249	-0.098	0.145	0.015	0.105
DFI_{740}	-0.026	-0.206	-0.077	0.186	0.093	0.149
EQY_{690}	0.108	-0.02	0.066	0.361	0.326	0.326
EQY_{720}	0.224	0.079	0.181	0.438	0.372	0.405
EQY_{740}	0.21	0.074	0.168	0.413	0.363	0.382
Rfd_{690}	0.003	-0.152	-0.045	0.287	0.224	0.245
Rfd_{720}	0.189	0.024	0.143	0.425	0.339	0.387

Rfd_{740}	0.189	0.032	0.142	0.418	0.349	0.382

Appendix C: Water stress photos

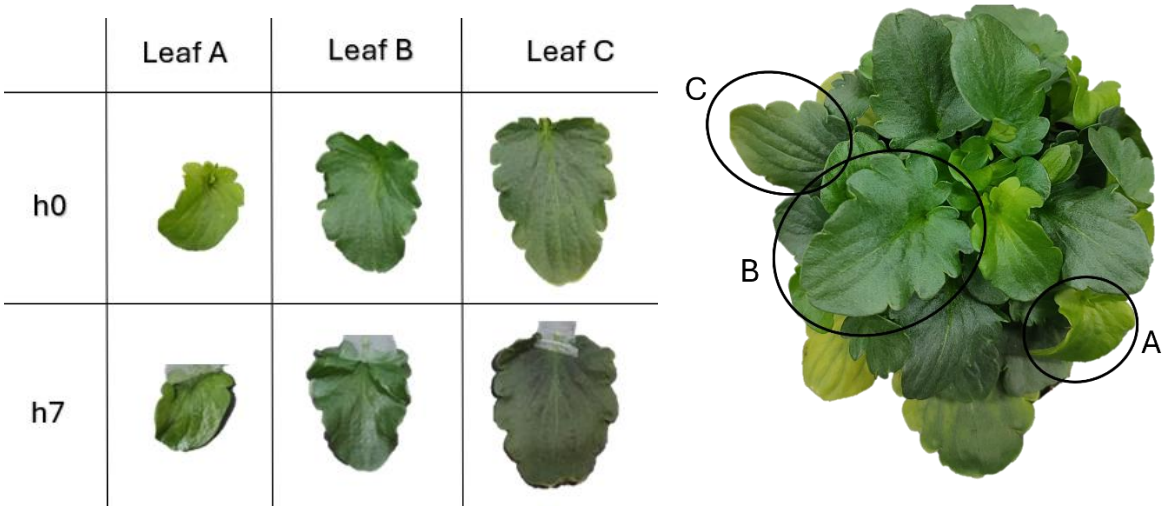

Figure C.0.1: Pictures of the detached leaves at hour 0 (h0) and hour 7 (h7) (left). The white parts at the top of the leaves for h7 is the tape that was used to attach the leaves to excite them. On the right, the placement of the leaves on *viola* 5 are marked, still attached to the plant.

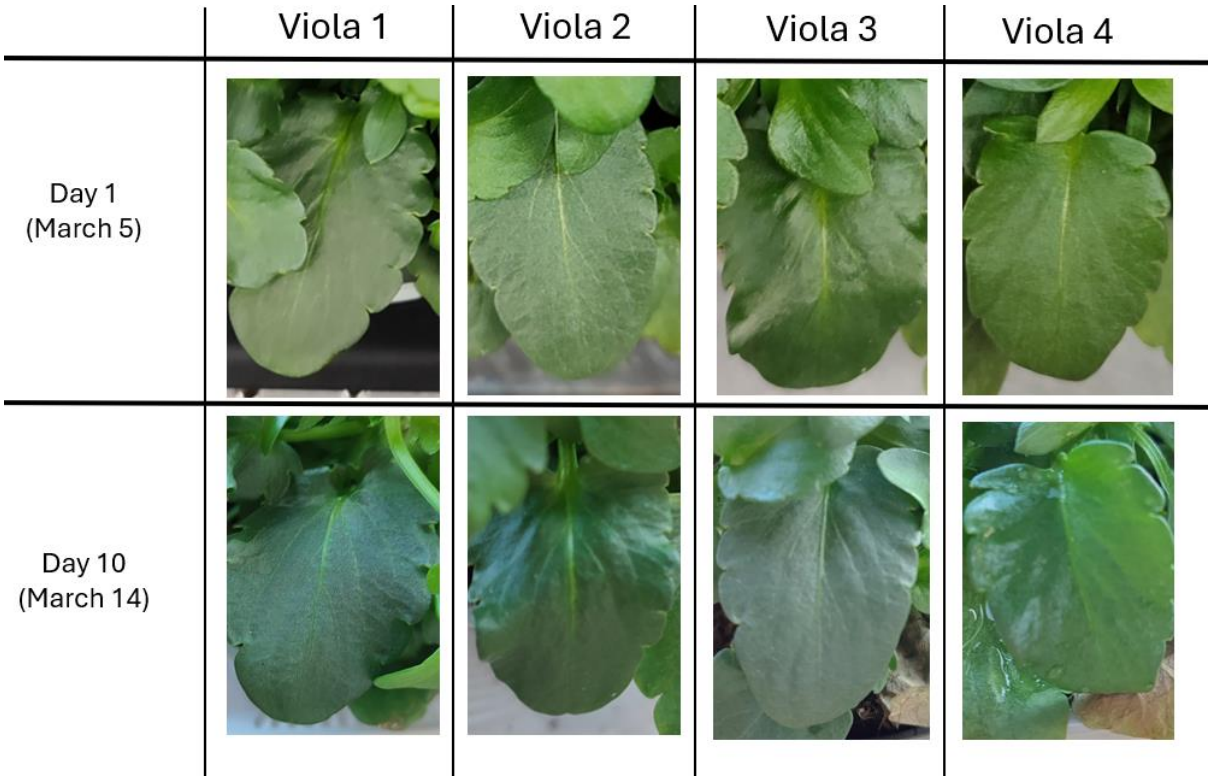

Figure C.0.2: Pictures of the excited leaves of slow stress experiment on leaf level. *Viola* 1 and *viola* 2 belong to the control group, *violas* 3 and 4 were subjected to stress.

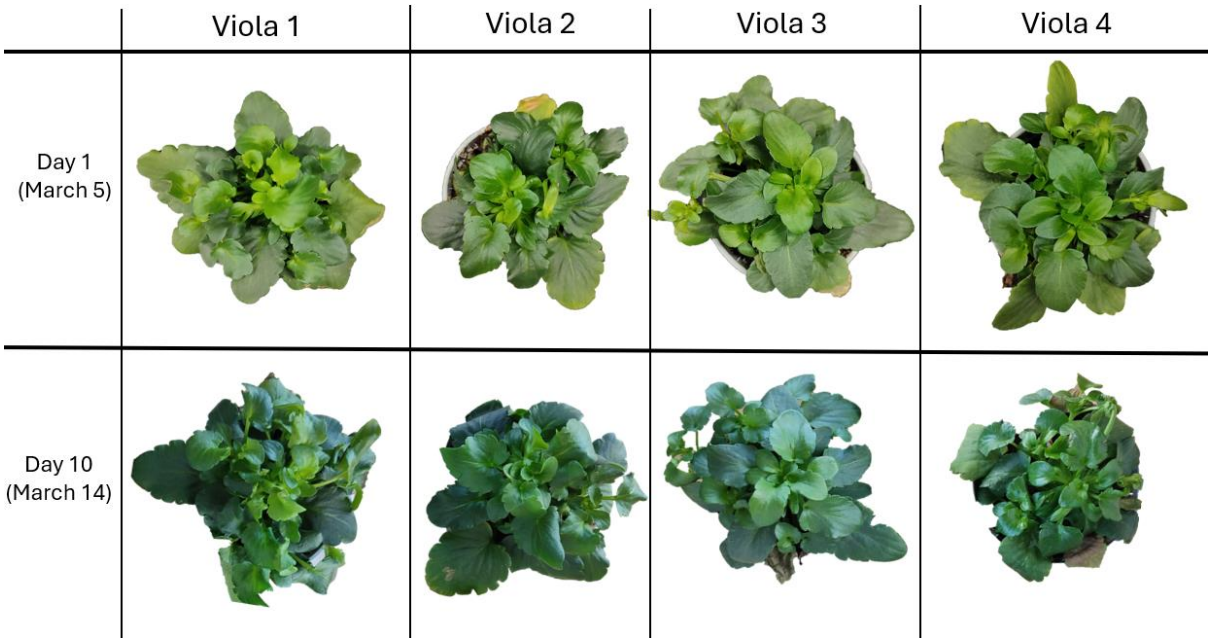

Figure C.0.3: Pictures of the plant at the first and last day of the slow stress experiment, at canopy level. *Viola* 1 and *viola* 2 belong to the control group, *violas* 3 and 4 were subjected to stress.

Appendix D: Water stress

Table D.0.1: Correlation and regression results for each leaf of the fast stress experiment between H% and F690/F730.

	r (Pearson)	formula	Adj. R-squared	p-value
Leaf A	0.910	Y = 0.78 + 0.004 X	0.799	0.0017
Leaf B	0.917	Y = 0.29 + 0.008X	0.814	0.0014
Leaf C	0.899	Y = 0.75 +0.004 X	0.776	0.0023

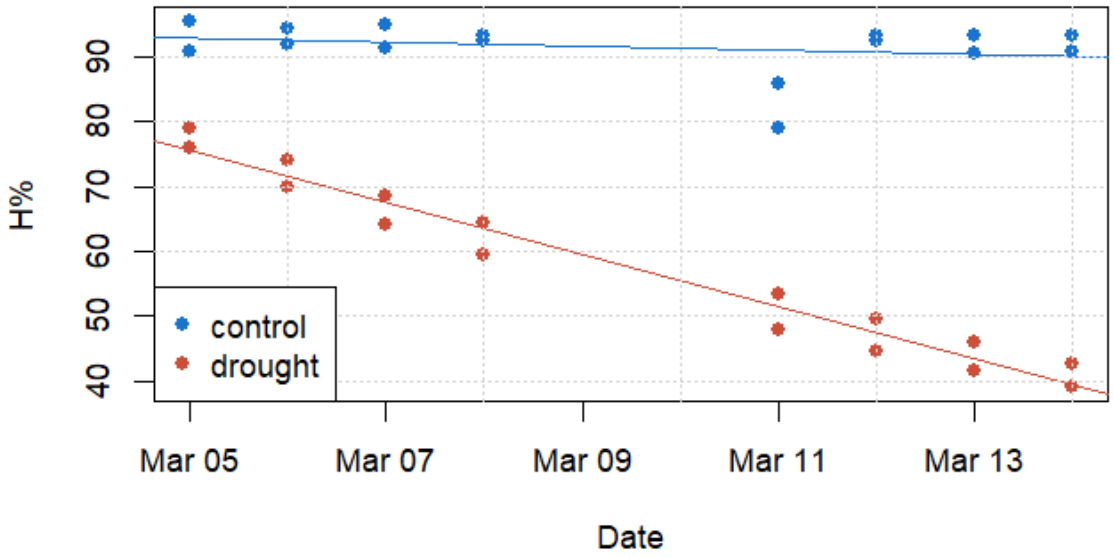

Figure D.0.1: Water content of control group (blue) and stressed group (red) over the duration of the slow stress experiment.

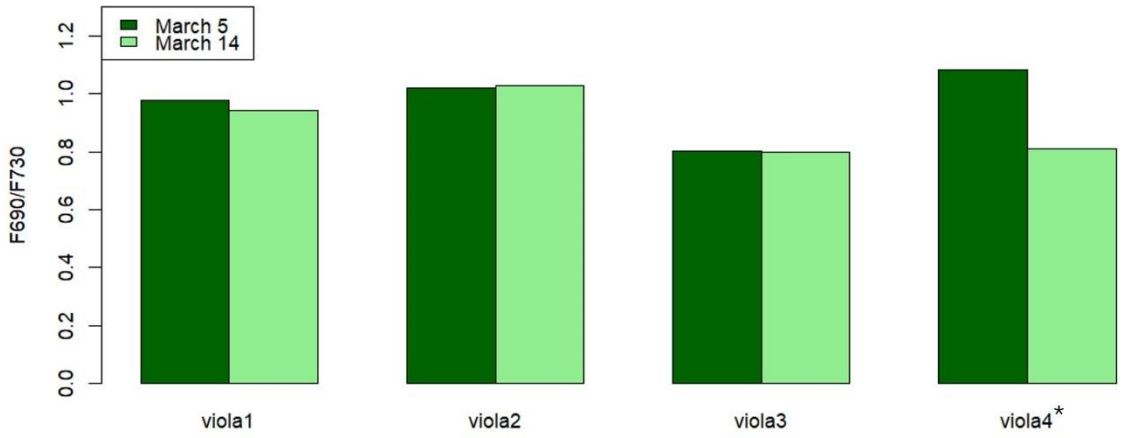

Figure D.0.2: Bar plot of the F_{690}/F_{730} values on leaf level for each plant recorded on the first and the last day of the experiment. For *viola* 1, 2, and 3, no significant difference was found. For *viola* 4 a significant difference was found, denoted in the figure with an asterisk (*).

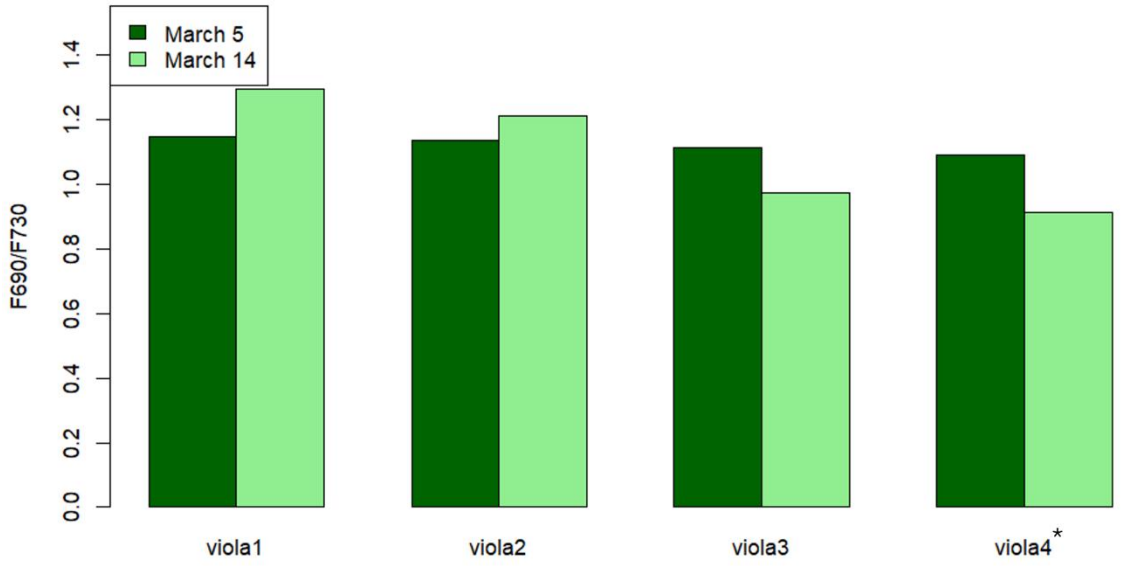

Figure D.0.3: Bar plot of the F_{690}/F_{730} values for each plant on canopy level, recorded on the first and the last day of the experiment. For *viola* 1, 2, and 3, no significant difference was found. For *viola* 4 a significant difference was found.

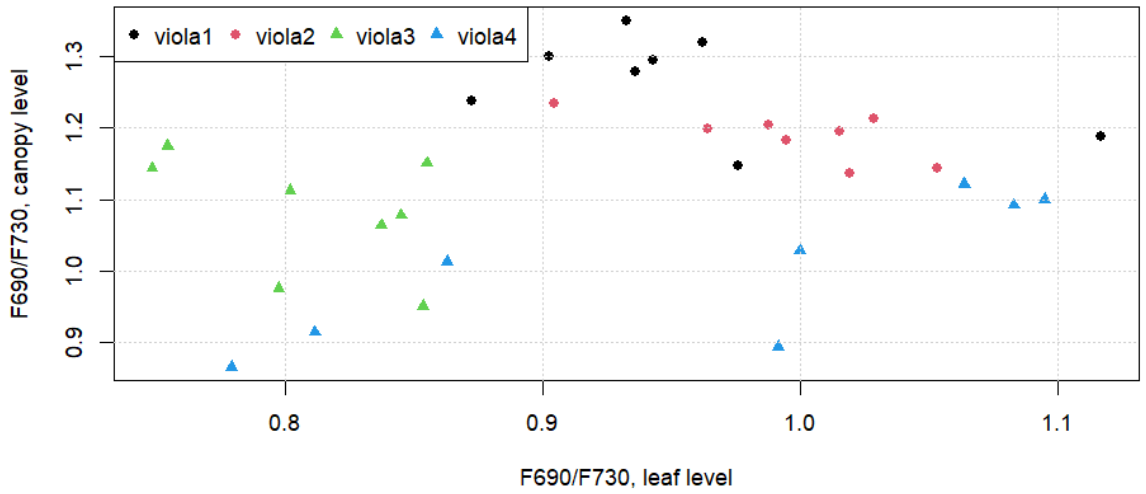

Figure D.0.4: Scatterplot of leaf level and canopy level fluorescence ratio F_{690}/F_{730}.